CP4O CCN - Development of a tidal atlas in the Arctic Ocean

Technical report

For the attention of: Dr Jérôme BENVENISTE - ESRIN/ESA

	Function	Name	Signature	Date
Prepared by	Project manager/ Project Team	Mathilde CANCET Ole ANDERSEN (DTU Space)		26/04/16
Approved by	Oceanography Business Unit Manager	Eric JEANSOU		26/04/16

NOVELTIS

153 rue du Lac – 31670 Labège – France
Tél. : +33 (0)562 88 11 11 – Fax : +33 (0)562 88 11 12 – E-mail : noveltis@noveltis.fr

Distribution list

INTERNAL	EXTERNAL	
Name	**Name**	**Company / Organisation**
Documentation NOVELTIS	Jérôme BENVENISTE	ESA/ESRIN
Richard BRU	David COTTON	SatOC
Cindy HORTALA	Ole ANDERSEN	DTU Space
Eric JEANSOU	Florent LYARD	LEGOS

Document status

CP4O CCN - Development of a tidal atlas in the Arctic Ocean Technical report			
Issue	**Revision**	**Date**	**Reason for the revision**
1	0	29/01/2016	Initial version
2	0	08/04/2016	Review from ESA
2	1	26/04/2016	Review from ESA

Modification status				
Issue	Rev	Status *	Modified pages	Reason for the modification
2	0	M	All pages	Review from ESA
2	1	M	All pages	Review from ESA

* *I = Inserted* *D = deleted* *M = Modified*

Acronyms

M2, S2, K2, N2	Tidal wave - semidiurnal constituents
K1, O1, P1, Q1	Tidal wave - diurnal constituents
M4, MS4	Shallow water overtide (non-linear components)
BLUE	Best Linear Unbiased Estimator
CEFMO	Code aux Eléments Finis pour la Marée Océanique (Finite Element Code for Ocean Tide)
CMEMS	Copernicus Marine Environment Monitoring Service
COMAPI	Coastal Modeling for Altimetry Product Improvement (regional tidal models)
CP4O	CryoSat Plus for Oceans (ESA project)
CryoSat-2	ESA mission for the study of the cryosphere including a SARin altimeter
DTU	Technical University of Denmark
DTU10	Global ocean tidal model from DTU
DTU13	Global mean sea surface based on 20 years of satellite altimetry, from DTU
DTU-LARS	Retracking System from DTU Space
Envisat	ESA satellite (2002-2012) including an altimeter
EOT11	Empirical Ocean Tide model (global tidal model)
ERS-1	ESA oceanography mission
ESA	European Space Agency
FES2004/2012/2014	Finite Element Solution (global tidal models)
GOT4.8	Goddard Ocean Tide (global tidal model from NASA Goddard Space Flight Center)
IBCAO	International Bathymetric Chart of the Arctic Ocean
JASON	NASA/CNES oceanography mission including an altimeter
LEGOS	Laboratoire d'Etudes en Géophysique et Océanographie Spatiales
LRM	Low Resolution mode
MSS	Mean Sea Surface
NSIDC	National Snow and Ice Data Center
RADS	Radar Altimeter Database System
R-Topo	Global bathymetry models
SAR	Synthetic Aperture Radar mode
SARAL/AltiKa	CNES/ISRO oceanography mission including the Ka-band AltiKa altimeter
SARin	Synthetic Aperture Radar interferometric mode
Sentinel-3	ESA oceanography mission including a SAR altimeter
SSH	Sea Surface Height

TOPEX	NASA/CNES oceanography mission including an altimeter
T-UGOm	Toulouse Unstructured Grid Ocean model
TPXO8	TOPEX/Poseidon Cross-Over Global Inverse Solution (global tidal model)

References

[RD1]	Stammer, D., et al. (2014), Accuracy assessment of global barotropic ocean tide models, Review in geophysics, DOI: 10.1002/2014RG000450
[RD2]	Cancet, M. et al. (2012), Latest improvements in tidal modelling: a regional approach, Proceeding of the 20 Years of Progress in Radar Altimetry Symposium, Venice, Italy
[RD3]	Lyard, F. et al. (2006), Modelling the global ocean tides: modern insights from FES2004, Ocean Dynamics 56, 394-415.
[RD4]	Carrère, L., Lyard, F., Cancet, M., Guillot, A., Roblou, L. (2012), FES2012: A new global tidal model taking advantage of nearly twenty years of altimetry, Proceeding of the 20 Years of Progress in Radar Altimetry Symposium, Venice, Italy.
[RD5]	Carrère, L., Lyard, F., Cancet, M., Guillot, A., Picot, N., Dupuy, S. (2015), FES2014: A new global tidal model, presented at the Ocean Surface Topography Science Team meeting, Reston, USA.
[RD6]	Cancet, M., Lux, M., Pénard, C., et al. (2010), COMAPI: New regional tide atlases and high frequency dynamical atmospheric correction, presented at the Ocean Surface Topography Science Team meeting, Lisbon, Portugal.
[RD7]	Radar Altimetry Database System RADS http://rads.tudelft.nl
[RD8]	Andersen, O. B., and R. Scharroo (2010), Range and geophysical corrections in coastal regions, book chapter in eds. (Vignudelli et al), Coastal altimetry, ISBN: 978-3-642-12795-3
[RD9]	Stenseng, L., "Polar Remote Sensing by CryoSat-type Radar Altimetry", Ph.d. Thesis, 2011 downloadable from space.dtu.dk
[RD10]	Cheng Y. and O. Andersen (2011), Multimission empirical ocean tide modeling for shallow waters and polar seas, Journal of Geophysical Research (ISSN: 0148-0227), DOI: http://dx.doi.org/10.1029/2011JC007172, vol: 116
[RD11]	Ge Chen and Hui Lin (2000), The Effect of Temporal Aliasing in Satellite Altimetry, Photogrammetric Engineering & Remote Sensing, Vol. 66, No. 5, pp. 639-644.
[RD12]	Andersen, O. B. (1994), Ocean tides in the northern North Atlantic Ocean and adjacent seas from ERS-1 altimetry, J. Geophys. Res., 99 (C11), 22557-22573.
[RD13]	Andersen, O. B. (1995), Global ocean tides from ERS-1 and TOPEX/POSEIDON altimetry, J. Geophys Res. 100 (C12), 25249-25259.
[RD14]	Andersen, O. B. (1999), Shallow water tides on the northwest European shelf from TOPEX/POSEIDON altimetry. J. Geophys. Res, 104, 7729-7741.
[RD15]	Andersen, O. B., Egbert, G. D, Erofeeva, L., and Ray R. (2006), Mapping nonlinear shallow water tides: a look at the past and future, Ocean Dynamics 56 (5), 416-429. DOI: 10.1007/s10236-006-0060-7
[RD16]	T-UGOm hydrodynamic model description: http://www.legos.obs-mip.fr/recherches/equipes/ecola/outils-produits/t-ugom-home-page
[RD17]	Le Bars, Y., Lyard, F., Jeandel, C., Dardengo, L. (2010), The AMANDES tidal model for the Amazon estuary and shelf, Ocean Modelling, vol. 31, Issues 3–4, 132–149, DOI:10.1016/j.ocemod.2009.11.001

[RD18]	Gill, A.E. (1982), Atmosphere-Ocean Dynamics, International Geophysics Series, Academic Press, vol. 30
[RD19]	Jakobsson, M., L. A. Mayer, B. Coakley, et al. (2012), The International Bathymetric Chart of the Arctic Ocean (IBCAO) Version 3.0, Geophysical Research Letters, DOI: 10.1029/2012GL052219.
[RD20]	Timmermann, R et al. (2010): Antarctic ice sheet topography, cavity geometry, and global bathymetry (RTopo 1.0.5-beta). doi:10.1594/PANGAEA.741917, Supplement to: Timmermann, R. et al. (2010): A consistent dataset of Antarctic ice sheet topography, cavity geometry, and global bathymetry. Earth System Science Data, 2 (2), 261-273, DOI:10.5194/essd-2-261-20100
[RD21]	Schaffer, J et al. (2016): Greenland and Antarctic ice sheet topography, cavity geometry, and global bathymetry (RTopo-2), links to NetCDF files. Dataset #856844 (DOI registration in progress), Supplement to: Schaffer, Janin; Timmermann, Ralph; Arndt, Jan Erik; Kristensen, Steen Savstrup; Mayer, Christoph; Morlighem, Mathieu; Steinhage, Daniel (2016): A global high-resolution data set of ice sheet topography, cavity geometry and ocean bathymetry. Earth System Science Data Discussions
[RD22]	Bennett (1992), Inverse Methods in Physical Oceanography. Cambridge University Press.
[RD23]	Lyard (1997), Data Assimilation in a Wave Equation: A Variational Representer Approach for the Grenoble Tidal Model, J. Computational Physics, Volume 149, Issue 1, 10 February 1999, Pages 1–31. DOI:10.1006/jcph.1998.5966
[RD24]	Echevin V., De Mey, P. and Evensen G. (2000), Horizontal and vertical structure of the representer functions for sea surface measurements in a coastal circulation model. J. Phys. Oceanog. 30: 2627-2635.
[RD25]	Evensen G. (2003), The Ensemble Kalman Filter: theoretical formulation and practical implementation, Ocean Dynamics 53: 343–367, DOI: 10.1007/s10236-003-0036-9
[RD26]	DTU10 Annual sea level model. ftp.space.dtu.dk/pub/DTU10.

Table of contents

List of Figures

List of Tables

1. Introduction

1.1. Context and objectives

In the context of the climate change, the Arctic Ocean is ever more becoming a region of interest, be it for geopolitical reasons, for transportation and trade evolutions, for oil and gas resources exploration and exploitation or for scientific studies.

The ocean tide is one of the main contributors to the ocean dynamics on the global ocean continental shelves. But if tidal modelling benefited from many improvements these last years (physics in the hydrodynamic models, mesh resolution, bathymetry improvement, assimilation of longer time series of satellite altimetry observations), even the most recent global tidal models still show errors on the continental shelves and in the regions where the tide is more complex to model, generally because of non-linear interactions between the tidal components [RD1]

This is particularly true in the Arctic Ocean, where the seasonal variations of the ice cover bring an additional difficulty to tidal modelling. In addition, the bathymetry is strategic information in this region and it is difficult to get access to high resolution sea floor data.

Figure 1 shows the performances of the most recent global tidal models in the Arctic Ocean, compared to tide gauge observations, for the main tidal component in the region, the M2 tidal wave. The sea ice cover seasonality was not accounted for in any of these models. However, it is likely that all these tidal models are closer to the “sea ice free” configuration, as the tide gauge and altimetry observations used for data assimilation or for optimal interpolation were mainly measured in sea ice free conditions. The vector differences between the models and the tide gauge observations are represented by red dots: the bigger the red dot, the larger the vector difference. The vector difference averaged over all the tide gauges is indicated by the value in blue in each plot.

As expected, the larger differences, corresponding to the larger errors in the models, appear on the shelves, in regions where the amplitude of the M2 tidal component is the largest and more complex to model.

Another important point about Figure 1 is the fact that all these models show equivalent performances even if they are based on different methods [RD1]. Indeed, the GOT4.8, DTU10 and EOT11 models are empirical models, based on an a priori global tidal model (FES2004) on which a layer of altimetry and tide gauge observations is applied through an optimal interpolation process. The FES2012/FES2014 and TPXO8 models are based on another method, which consists of a hydrodynamic simulation with data assimilation. The same method was used to implement the FES2004 older tidal model. The model that obtains the best results is the FES2014 global model but it should be noticed that part of the tide gauge data assimilated in this model is used for the comparison, so the exercise is biased (regarding FES2004 and TPXO8 as well, but they obtain lower results than FES2014).

The objective of this extension of the CP4O project was to implement a regional tidal model in the Arctic Ocean in order to provide a better solution than the current global models in this region [RD2]. This model was developed following the same strategy as for the FES2012 and FES2014 global tidal models, i.e. using a hydrodynamic model with data assimilation. In addition to a high resolution mesh and a regional tuning of the hydrodynamic model, this regional model benefited from the availability and the recent reprocessing of CryoSat-2 altimetry data in the Arctic Ocean, besides Envisat data.

The report describes the methodology used to implement this regional model and the performances obtained against the available validation databases.

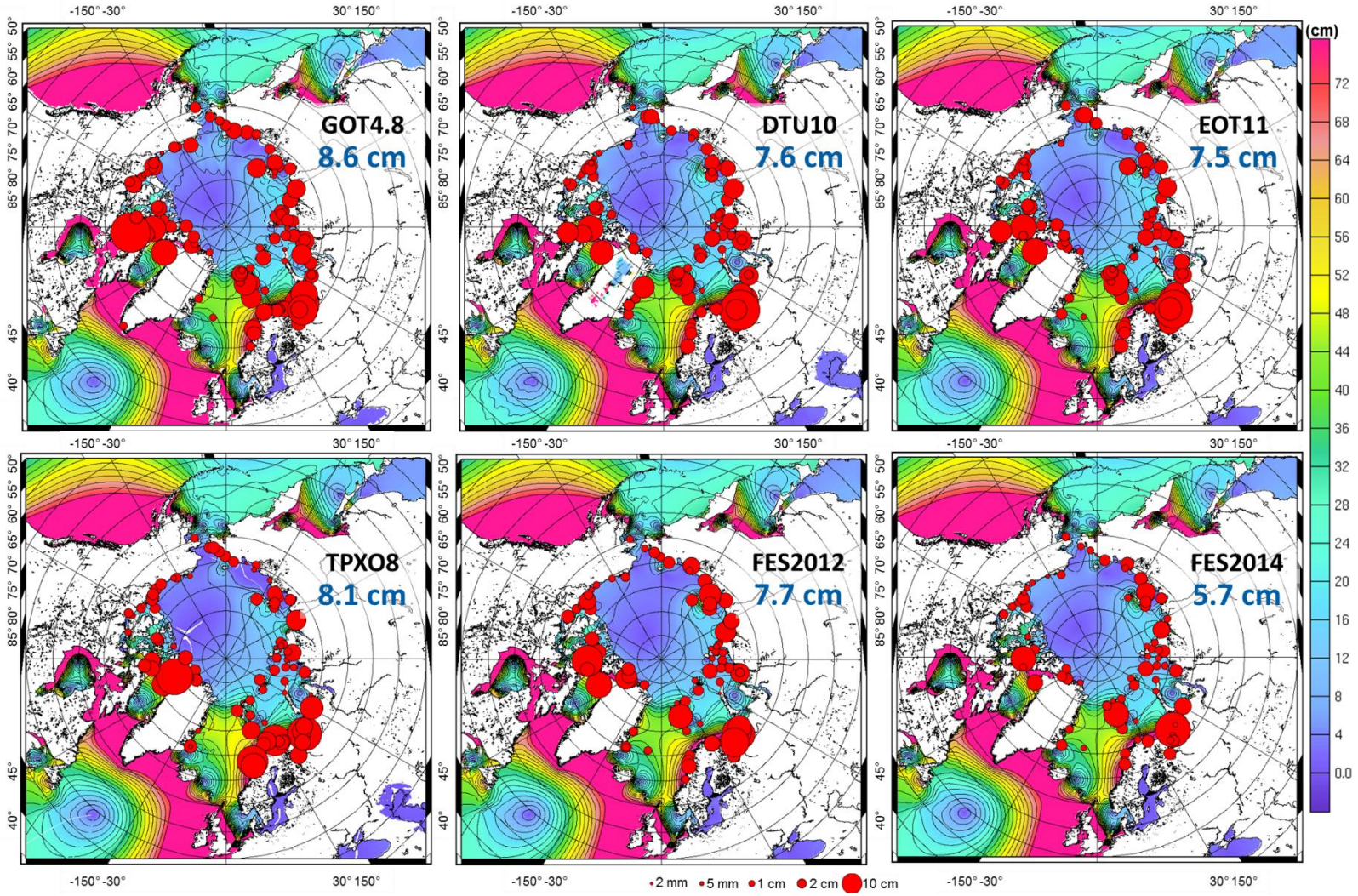

Figure 1: Vector difference between the global tidal models and the tide gauge stations for the M2 tidal component in the Arctic Ocean. The value given in blue is the mean vector difference over all the stations. The background colour map is the amplitude of the M2 tidal component from the models (in cm).

1.2. Main results

1.2.1. Performances of the Arctic tidal atlas

As will be evidenced from the following, the validation results demonstrate the high accuracy of the Arctic tidal atlas compared to the most recent global tidal atlases, when the differences are significant.

Some additional and independent validation activities will be performed to assess the quality of this regional tidal atlas.

We recommend to use the model “as is” for ocean modeling and forecasting in the Arctic Ocean. It can also provide an improved tidal correction in the CryoSat-2 ocean products, and for altimetry missions with high-inclination orbits, such as Envisat, SARAL/AltiKa and Sentinel-3. The new atlas can also benefit to the Copernicus Marine Environment Monitoring Service (CMEMS), which includes the Arctic Ocean as one of five priority European regional seas, and to other European Arctic observing systems.

Finally, as the Arctic tidal model was built on the basis of the FES2014 global tidal model (FES2014 tidal boundary conditions and regional improvement of the resolution of the FES2014 global mesh), it is possible to integrate the regional model into the global one and thus obtain a global model with an improved solution in the Arctic Ocean, with perfect match at the boundaries thanks to the unstructured mesh.

1.2.2. Possibilities of improvements

The implementation of the Arctic tidal atlas raised a number of questions regarding the quality of the data used as inputs (bathymetry, coastline, altimetry and tide gauge data) and the physics in the hydrodynamic model. Some possibilities of further improvements have been identified, which could not be implemented or tested in the framework of this study, due to the project planning, the manpower allocation and the availability of the datasets.

- The analysis of the purely hydrodynamic solution (no data assimilation) showed that the performances of the main diurnal components (K1 and O1) are lower than the performances of the semi-diurnal components. Some possible solutions for model improvement have been identified by the team that develops the model at LEGOS, but they would demand some time and some further thinking to be implemented. These lower performances have been corrected through the data assimilation process, by constraining the model to be close to the altimetry and tide gauge observations, but having the best hydrodynamic solution prior to data assimilation would be preferable, in particular in a region where the assimilated observations are scarce and sometimes dubious.
- DTU Space identified a source of improvement in the processing of the altimetry data for tidal analysis, regarding the diurnal components that were not optimally estimated (particularly K1 and P1) because of the problem of the alias periods for the major diurnal constituents in the Envisat sea surface height data. Another source of improvement of the altimetry data would be the computation of error estimates at each point that would help to select the most accurate data.
- The bathymetry quality is a crucial point for tidal modeling and the Arctic Ocean is a very complex region on this aspect. The comparisons between two different datasets (IBCAO and R-Topo) in the frame of this project showed that they both contain errors. A new version of the R-Topo bathymetry was very recently released, but it was not possible to test it in the framework of this study due to the agenda. A complementary approach could consist in designing a specific bathymetry dataset based on these various sources of data. Another strategy could also be the inversion of altimetry data, given the fact that many observations are now available at the high latitudes thanks to the CryoSat-2 mission.

It should be noticed that even if some of these possibilities of improvements demand some developments, this CP4O CCN project was the occasion to automate some tools, such as the mesh generation tools, and to set-up the hydrodynamic model in this specific region. This means that implementing these improvements would not necessarily request to redo the whole work.

2. Methodology and results

2.1. Description of the methodology

The regional tidal model implemented by NOVELTIS in the Arctic Ocean is based on the same methodology as the one used to implement the global tidal models FES2004 [RD3], FES2012 [RD4] and FES2014 [RD5], and the COMAPI regional models [RD6] in the Mediterranean Sea and in the North-East Atlantic Ocean (CNES projects).

Figure 2 shows the generic strategy followed by NOVELTIS to implement tidal models and, in particular, regional ones. The various steps of this method are described rapidly in this section and are more detailed in the following paragraphs, for the specific case of the Arctic Ocean.

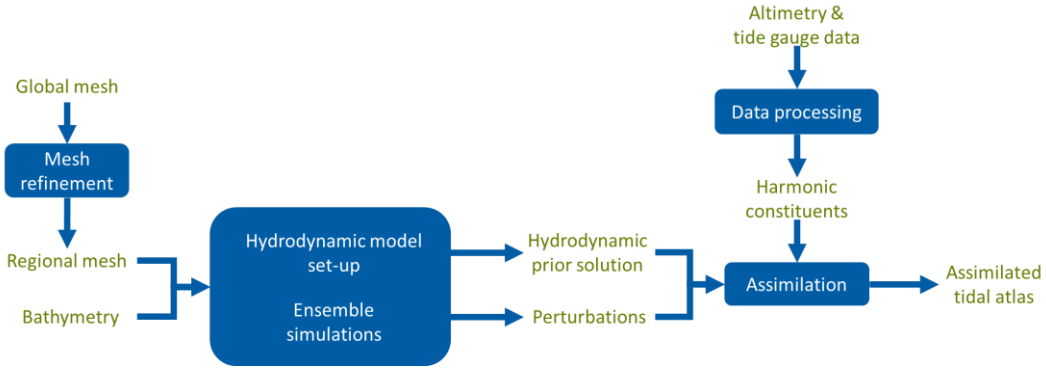

Figure 2: Diagram of the methodology followed by NOVELTIS to implement a regional tidal model.

- **Mesh refinement:**
  Thanks to the limited size of the region of interest, compared to a global model which can lead to computational limitations in terms of memory and speed, the grid resolution of a regional model can be refined in order to be able to model the non-linear structures and the local dynamical constraints with a good accuracy.

- **Hydrodynamic model set-up:**
  The quality of the tidal atlas highly depends on the tuning of the physical parameters of the hydrodynamic model. For example, the bottom friction accounts for the energy losses induced by the friction of the fluid on the ocean floor. It is thus related to the floor characteristics (shape, roughness), to the fluid characteristics (viscosity) and to the flow features (water height, velocity) and must be tuned as to give a realistic picture of the tidal energy dissipation. Generally, a unique value is chosen for the entire model (global or regional), which means that it is a compromise between what happens in the deep ocean and in the shelf seas, where the friction is stronger. As a consequence, the unique value chosen for this parameter in the case of a global model is likely to be less representative of the local ocean dynamics than the value chosen for a regional model [RD2].

- **Ensemble simulations:**
  The data assimilation strategy used by NOVELTIS is based on the ensemble method (see §2.5.1 for more details on the methodology). The analysis of the hydrodynamic model errors, due to the main parameters to which the model is sensitive, is done by varying these parameters in a range of values, in sub-domains representative of the model dynamics (areas of highest dissipation due to a given parameter). The variability of the ensemble of these various simulations gives a geographical picture of the model sensitivity to these parameters, and of its associated errors. This highlights the regions where the data assimilation could improve the model.

- **Data assimilation:**
  The data assimilation method calls representer functions based on the hydrodynamic prior solution (reference solution), the ensemble simulations (repartition of the model errors) and the observations to be assimilated. These observations are tidal harmonic constants derived from altimetry and tide gauge sea surface height time series. The best solution obtained through the data assimilation process is the final assimilated tidal atlas, also called **optimal tidal atlas**.

2.2. Altimetry data processing

The tidal harmonic constants (amplitude and phase lag) used for the validation and the assimilation in the Arctic tidal model were derived from tide gauge and altimetry observations (Figure 2). The tide gauge data were provided by LEGOS and consist of the collation of various historical databases from international programs as well as Canadian and Russian sources. The altimetry data were processed by DTU Space specifically for this CP4O CCN project.

2.2.1. Altimetry missions and products

The following satellite altimetry missions were processed:

- CryoSat-2 data in LRM mode (2010-2014), from 55°N to 88°N;
- Envisat data (2002-2010), from 55°N to 82°N;
- CryoSat-2 data in SAR and SAR-in mode (2010-2014), from 55°N to 88°N.

The CryoSat-2 data in LRM mode as well as the Envisat data were taken from the RADS data archive [RD7], using the state of the art range corrections as detailed on [RD7] and in [RD8].

The Cryosat-2 data in SAR and SAR-in modes in the Arctic Ocean were retracked in-house using the primary peak retracker from the DTU-LARS retracking system [RD9].

No ocean tide correction was applied to the altimetry data during this processing.

The RADS data were extracted using a custom-made editing selection for Polar Ocean use. This specific editing is based on the results of [RD10], which showed that a high number of good sea surface height observations in RADS is rejected because the default editing rejects the sea surface heights corresponding to significant wave heights lower than 0.1 meter. The specific Polar Ocean editing retrieves roughly twice as much altimetry data in the Arctic Ocean compared to the default editing in RADS. As we partly by-pass the normal editing, an a posteriori editing must be performed. This was done by editing the SSH data with respect to a 50 cm threshold to the DTU13 MSS, in order to remove possible outliers [RD10]. The resulting dataset showed no increased standard deviation compared to the standard edited RADS dataset.

The determination of the tidal constituents was performed through a remove/restore methodology [RD8]. Here, the FES2004 geocentric tide was removed from the altimetry SSH prior to tidal prediction in order to remove the known tidal signal and in particular the small scale signals that are not fully resolved with satellite altimetry. Then the tidal analysis was performed on the de-tided altimetry data and subsequently the FES2004 harmonic constituents were added/restored to the estimated harmonic constituents to obtain the final full tidal signal.

2.2.2. Response method for tidal analysis processing

With a repeat period of 369 days, the alias periods of most tidal constituents are far longer than the duration of the CryoSat-2 mission, as shown in Table 1. Hence it is not possible to apply tidal analysis at each co-linear point of the CryoSat-2 altimeter ground-tracks for estimating the ocean tide as it is generally done for missions with shorter repeat periods (Topex/Jason suite for example). For Envisat also, the direct estimation of the S2 tidal component is not possible due to the infinite alias period (see Table 1 and [RD11]).

Table 1: Alias periods for the main tidal components, for the CryoSat-2 and Envisat repeat periods.

Mission	M2	S2	K1	O1
CryoSat-2	112 years	Infinite	90 years	60 years
Envisat	95 days	Infinite	1 year	75 days

Another reason for not applying co-linear analysis is the fact that a large amount of data is missing or less accurate in the Arctic Ocean, in particular because of the seasonal sea ice cover. In addition, Envisat and CryoSat-2 do not have similar ground-tracks.

For all these reasons, CryoSat-2 and Envisat are in orbits that hamper the use of a harmonic method for tide prediction [RD12]. Consequently we decided to adapt the response formalism for tidal prediction in this project. Instead of using co-linear analysis, we applied a technique in which all tracks within a given region were used to predict the residual tidal constituents.

First, an Arctic grid of 1°x3° (optimal based on experiments) was used to select the altimetry data (Figure 3).

For each crossing of each pass of each satellite, the averaged latitude, longitude, time and sea surface height (SSH) *h(t)* for that particular crossing is computed and the averaged SSH is saved for the subsequent tidal analysis.

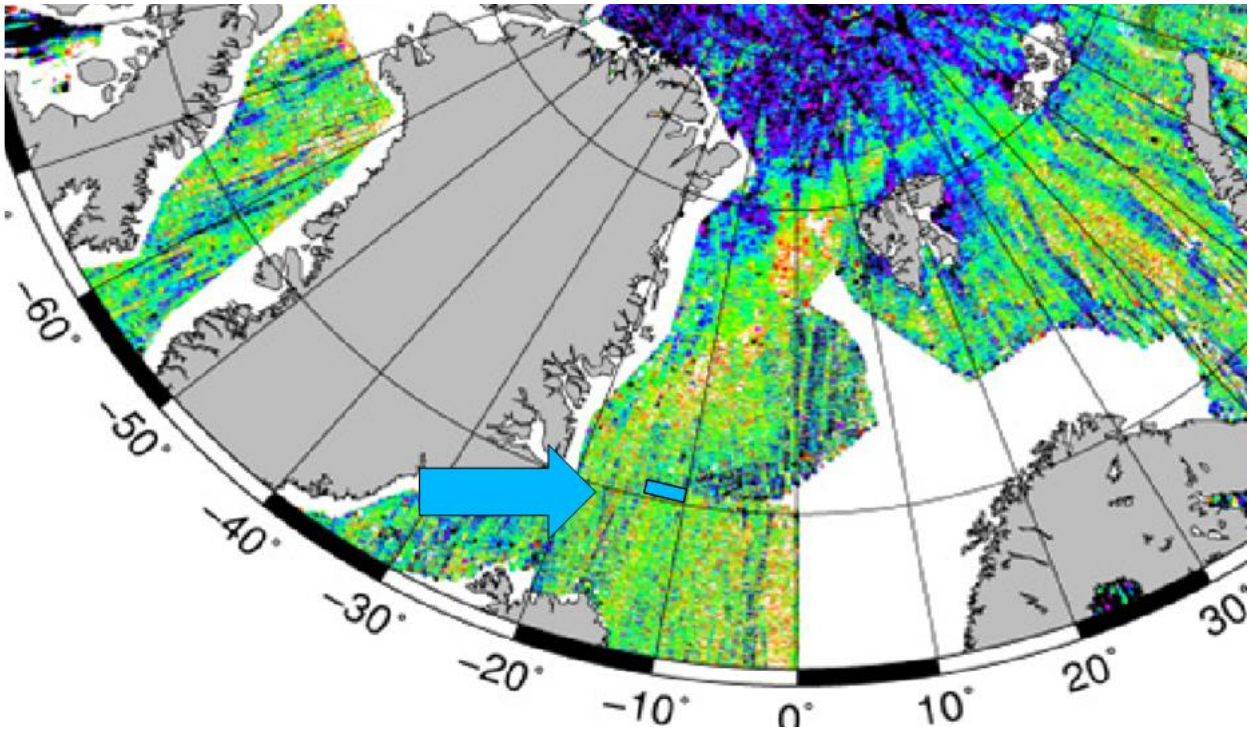

Figure 3: Illustration of one of the 1 x 3 degree boxes in the Arctic Ocean used to gather the height of all the altimeter crossings.

The compiled set of all the altimeter observations was analysed using the "response method" [RD13] for the remaining semidiurnal and diurnal constituents, supplemented with harmonic analysis methods for the two largest shallow water non-linear constituents (M4 and MS4, not provided afterwards) as well as the annual variation in sea level. This results in the following formalism relating the observational heights *h(t)* to the unknown parameters ([RD14] and [RD15]):

$$h(t) = \sum_{m=1}^{2}\sum_{k=-K}^{K}[u_k\, a^m(t-\Delta k) + v_k\, b^m(t-\Delta k)] \quad \text{(diurnal, semidiurnal)}$$
$$+ \sum_{n=1}^{N}[H1_n \cos(\sigma_n t) + H2_n \sin(\sigma_n t)] \quad \text{(shallow water)} \qquad \text{(eq.1)}$$
$$+ H1_{ann} \cos(\sigma_{ann} t) + H2_{ann} \sin(\sigma_{ann} t) \quad \text{(annual variation)}$$

where $a^m(t-\Delta k)$ and $b^m(t-\Delta k)$ are the real and imaginary components of the time-varying part of the tide-generating potential associated with each band and lagged by Δk days. The unknown coefficients sought are u_k and v_k for the diurnal and semidiurnal constituents, respectively, and $H1_n$ and $H2_n$, the coefficients for each shallow water constituent of frequency σ_n. Finally, $H1_{ann}$ and $H2_{ann}$ are the coefficients for the annual variation of frequency σ_{ann} = 1/365 days [RD13]. Subsequently, the response parameters (u_i, v_i) are turned into tidal constituents. These harmonic constituents as well as the shallow water constituent parameters are corrected by 8% to account for the residual loading effect of the residual geocentric tide estimated in the response solution. Finally the FES2004 ocean tide constituents were interpolated onto the location of the cells and the ocean tide signal from this model was restored in order to obtain the final altimetry-derived tidal constituents (Figure 4).

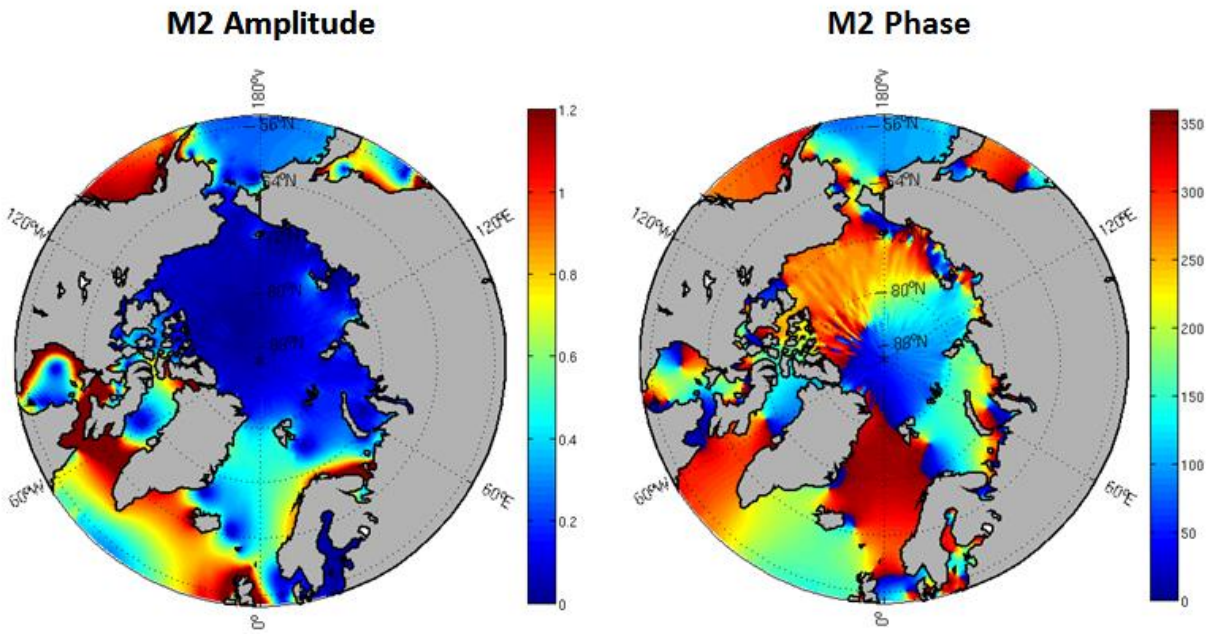

Figure 4: The M2 tidal constituents (amplitude in meters and phase in degrees) derived from satellite altimetry in the Arctic Ocean, interpolated to a regular grid for the entire Arctic Ocean.

2.2.3. Validation

Initially, a comparison with tide gauges was performed for the altimetry-derived tidal constituents to make a sanity check on these (Figure 5). It is important to note that the altimetry-derived tidal constituents are only available on a relatively coarse grid (1°x3°). Hence they will not be comparable in accuracy to most global ocean tide models if the comparison is performed between the points of this 1°x3° grid. At the points of the grid, the altimetry-derived tidal constituents are comparable to the ocean tide models in terms of accuracy. They will be assimilated into the regional Arctic Ocean tidal model at these specific locations.

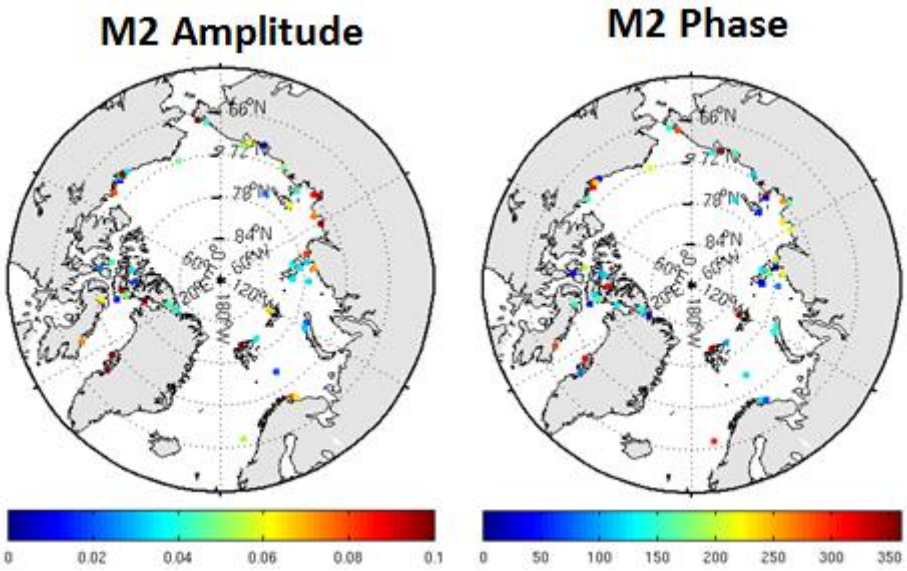

Figure 5: Residuals between the altimetry-derived ocean tide constituents and the tide gauge-derived tidal constituents for amplitude (in meters) and phase (in degrees) of M2. The figure is similar to the comparison figures in [RD1]

2.2.4. Concluding remarks

Although the tidal constituents derived from satellite altimetry are comparable in accuracy to ocean tide models like FES2004, we have realised that the approach we applied in this analysis is not optimal for tidal analysis in the sense that we simultaneously solve for the annual signal together with the response parameters. Indeed, in large parts of the Arctic Ocean the amplitude of the annual variation is larger than 5-10 cm and hence comparable to some tidal constituents.

We thought that the presence of a large amount of CryoSat-2 data would have enabled the discrimination between the annual variation in the sea level and the problem of annual alias periods for the major diurnal constituents for the Envisat sea surface height data (in particular K1, see Table 1). However, the phase of the diurnal constituents apparently changes so slow for CryoSat-2 that this large amount of data does not really help to solve this alias problem and the derived constituents for several diurnal constituents (particularly K1 and P1) are not optimally estimated.

It is our conclusion that it would have been better to initially remove the annual variation in the sea level and then use the cleaned signal (better representing the tidal variation in sea level) to estimate the ocean tide parameters, as done in [RD10]. However, the estimates for the semi-diurnal tidal constituents are not impacted by this issue and should enable to provide accurate assimilated solutions, in particular for M2, the main tidal component in the Arctic Ocean.

2.3. Hydrodynamic simulation

As shown in Figure 2, the first steps in the implementation of the Arctic Ocean tidal model consist in generating a hydrodynamic simulation of the ocean tides that will be considered as the reference for the data assimilation process. The implementation of this hydrodynamic solution is based on the T-UGOm hydrodynamic model [RD16].

2.3.1. T-UGOm hydrodynamic model

The T-UGOm model (Toulouse Unstructured Grid Ocean model) is an unstructured grid 2D/3D hydrodynamic model developed at LEGOS (Laboratoire d'Etudes en Géophysique et Océanographie Spatiales) [RD17]. The 2D equations of the model are based on the classical shallow-water equations of continuity and movement. It can be run using the finite elements discretization, with triangular elements. The unstructured grid enables to easily increase the resolution in the most demanding parts of the model, in terms of coastal geometry and/or hydrodynamic constraints. It is of particular interest in areas of steep topographic gradients, where the currents generally show high variability and internal waves are generated, as well as in the shallow waters, where the energy dissipation is the highest due to the bottom friction.

In the case of tide simulation, two modes are available to solve the equations.

The time-stepping mode consists in running the model over a given period, long enough (generally one year) to be able to discriminate the various tide waves with good accuracy. The equations of the ocean dynamics are integrated over the time with a time step adapted to the grid resolution and to the tide propagation. Once the simulation is achieved, a harmonic analysis is performed on the sea surface elevations generated by the model, in order to compute the harmonic constituents (amplitude and phase) of the tide components. This method enables to model the non-linear tide components following the natural process of dynamical interactions between the various components of the spectrum. This mode is also able to deal with wetting and drying flats, and with river discharge.

The spectral mode, initially inspired by the CEFMO (Code aux Eléments Finis pour la Marée Océanique) code used to compute the FES2004 reference tidal atlas [RD3], solves the quasi-linearized Navier-Stokes equations [RD18] in the spectral domain, in a wave by wave, iterative process. This mode is very well adapted to compute the waves resulting of the astronomical forcing, whereas it is more complex for the non-linear components, which are better resolved with the time-stepping mode. However, the iterative process enables to solve the non-linear tides with a sufficient accuracy in most cases. The run duration is drastically reduced with the spectral mode (a few minutes to a few hours depending on the mesh), compared to the time-stepping mode that would require several days.

2.3.2. Validation method and databases

The T-UGOm hydrodynamic model provides tidal outputs that consist of one NetCDF unstructured file per tidal component containing the amplitude and phase lag of this component at each point of the grid. It is consequently possible to evaluate the performance of the model for each tidal component, by comparing its tidal harmonic constituents (amplitude and phase lag) to the tidal harmonic constituents extracted from the harmonic analysis of tide gauge and satellite altimetry observations time series, in terms of amplitude differences, phase lag differences and vector differences.

Regarding the satellite altimetry observations, we used the dataset provided by DTU Space, both for validation and data assimilation activities.

Regarding the tide gauge observations, they were provided by LEGOS and consist of a compilation of various data sources gathered throughout the years. Some of them come from old datasets (such as some Russian tide gauges from the 1980s). Some of them have dubious locations (on the ground), some of them have clear clock errors (local time). Some of them only have a few tidal components. For most of them, the elevation time series are not available, which means that the harmonic analysis cannot be run again and cross-checked.

All these points lead to the conclusion that not too much confidence should be put into this tide gauge dataset if it is not strictly edited. This is the reason why a strict editing of this database has been performed by NOVELTIS and LEGOS for years, leading to the constitution of a validation dataset of 121 tide gauge stations.

2.3.3. Mesh refinement

Instead of starting from scratch, the unstructured mesh in the Arctic Ocean is based on the existing FES2014 global model grid (Figure 6). This strategy was chosen because it makes it possible to patch the regional model in the global one, if necessary. Indeed, the unstructured elements at the boundaries of the regional mesh are consistent with the global mesh elements.

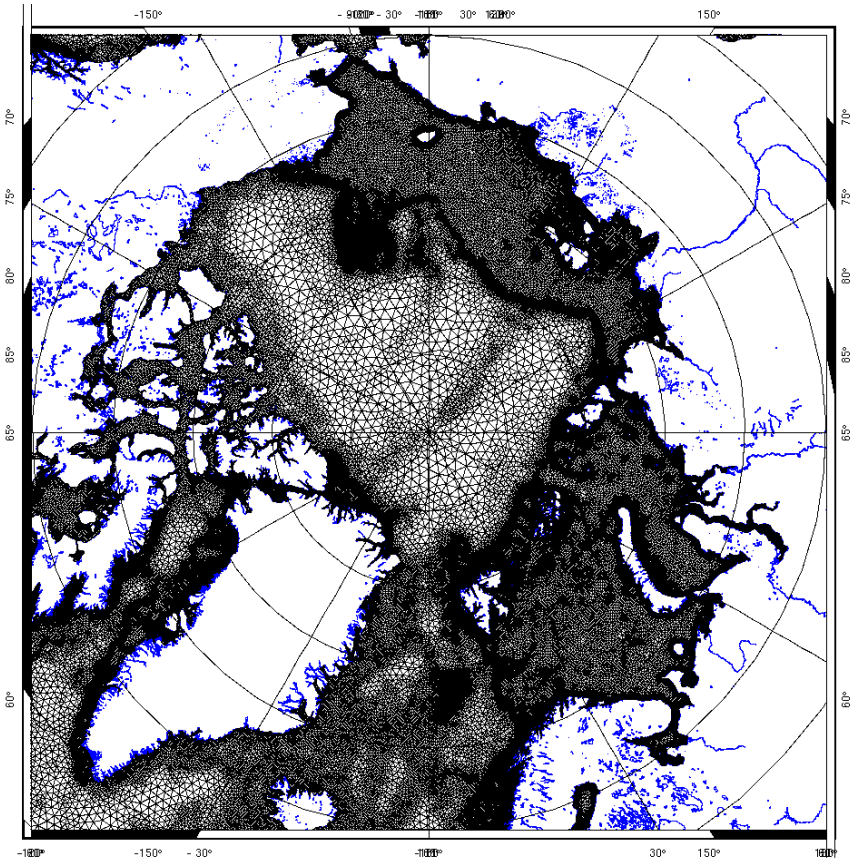

Figure 6: Unstructured mesh of the FES2014 global model in the Arctic Ocean.

The global mesh resolution was locally increased using a set of tools developed by LEGOS. Given the complexity of the coastline in the Arctic region, many peculiar cases were encountered during the application of these tools, which led to many improvements in order to automate the tools as much as possible. Today, it is possible to generate a high resolution unstructured mesh in a very complex region within a few hours thanks to this set of tools.

Figure 7 shows the local refinement of the mesh resolution in the North West Passage. For this example, the resolution of the FES2014 initial mesh ranges from 15 km at the coast to about 25 km offshore, whereas for the refined mesh, the resolution is 4 km along the coast (and even finer locally, down to 500 m, around some islands) and about 8 km offshore.

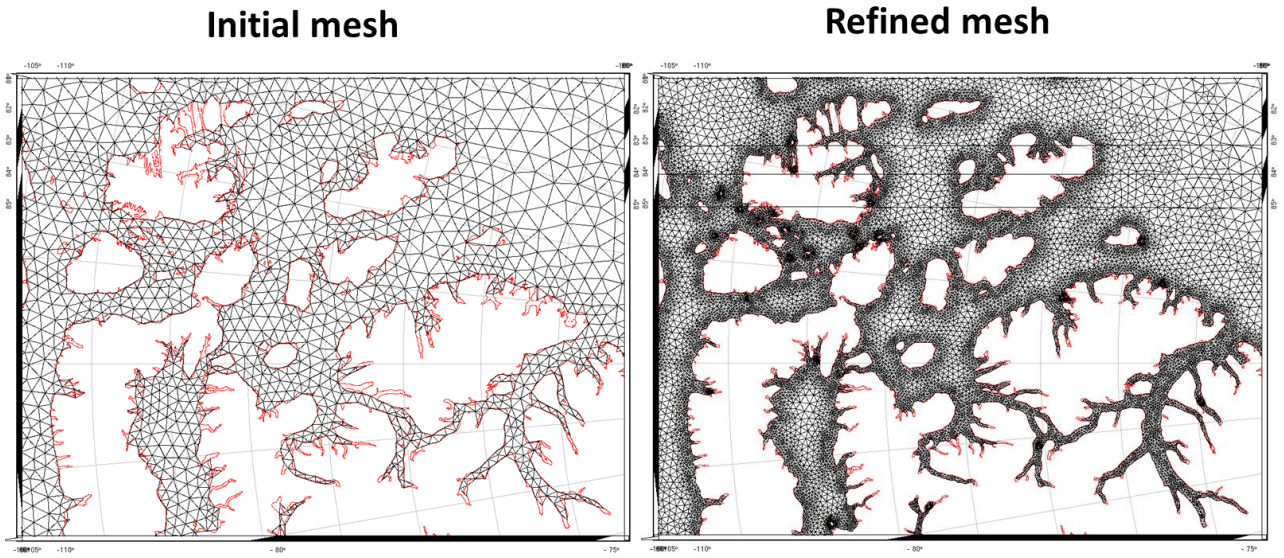

Figure 7: Zoom on the initial and refined unstructured meshes in the North West Passage.

Over the whole Arctic Ocean, the resolution of the refined mesh has been set to 4 km all along the coast, with local refinements down to a few hundreds of meters, and reaches a maximum of 40 km offshore (to be compared with more than 80 km offshore for the initial FES2014 mesh), as shown in Figure 8.

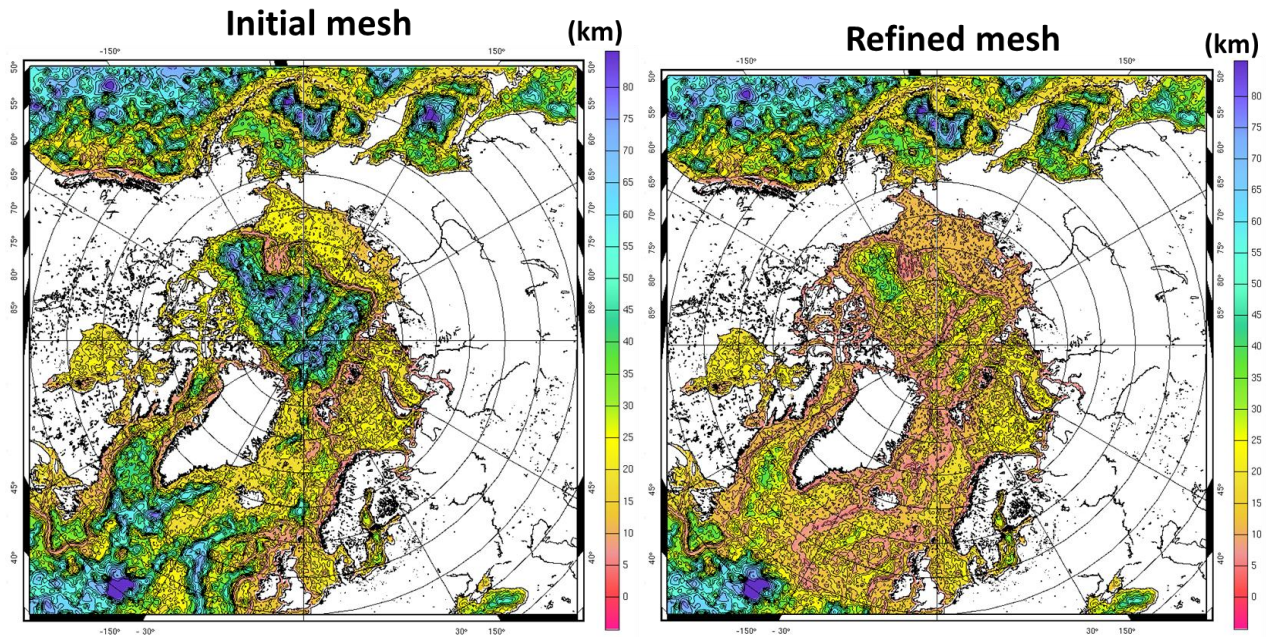

Figure 8: Resolution (in km) of the initial and refined meshes in the Arctic Ocean.

Finally, the Arctic region was extracted from the refined global mesh, which gave the regional mesh illustrated in Figure 9. The open ocean boundaries were chosen as such to benefit from the assimilation of Topex/Jason data in the global model used as boundary conditions (i.e. under 66°N) , but also in order to avoid some complex tidal structures that would not be well solved in the global model, in particular between Iceland and Scotland.

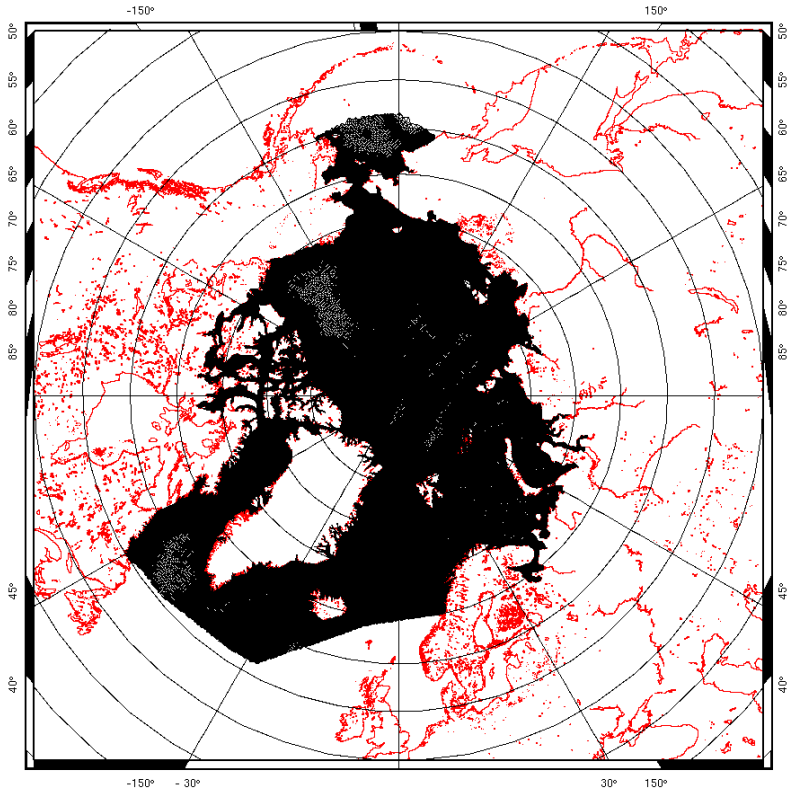

Figure 9: Final regional mesh over the Arctic Ocean (to be compared to Figure 6).

The final refined regional mesh is composed of 268 218 vertices, while the FES2014 global mesh has 88 271 vertices over the same region and 797 366 vertices in total. These numbers show the large improvement made to the mesh resolution in the Arctic Ocean. However, it is very difficult to establish a direct link between the mesh resolution and the expected accuracy of the tidal model, because of possible compensations between model errors due to a lack of resolution and bathymetry errors.

2.3.4. Bathymetry

The accuracy of the tidal model highly depends on the quality of the bathymetry data used as an input of the hydrodynamic model. In particular, the tidal processes interact with the bathymetry in the shallow water regions, which leads to the generation of non-linear tidal components. Errors in the bathymetry can consequently have large consequences on the model results and performances.

The Arctic Ocean is a region of more than 14 billion km², partly covered with sea ice throughout the year, with large seasonal variations in the sea ice cover. This means that it is complex to measure accurate bathymetry information in the whole region. In addition, it is a highly strategic region for commercial activities and geopolitical reasons, which means that the high resolution observations, when they exist, are generally not widely distributed even for scientific exploitation.

The bathymetry dataset most commonly used for scientific studies in the Arctic Ocean is the IBCAO grid (International Bathymetric Chart of the Arctic Ocean), an international initiative that provides bathymetric data on a 500 meter spacing [RD19]. Timmerman et al. have also developed the R-Topo global bathymetry with some improvements at the poles, using multibeam survey data [RD20].

Both bathymetry datasets have been tested by NOVELTIS during the implementation of the Arctic tide model, in order to choose the dataset that would prove the most appropriate. Figure 10 shows the performances of the hydrodynamic model towards the tide gauge stations (see the next section for the details about the model set-up and validation), for each bathymetry dataset and for the M2 tidal component. The larger the red dot, the larger the vector difference to the tide gauge station. The largest difference between the two simulations is located in the South of Greenland, where the model based on the R-Topo bathymetry shows a vector difference of more than 40 cm at the Qaqortoq tide gauge station, when the difference is of only a few centimeters in the case of the model based on the IBCAO bathymetry.

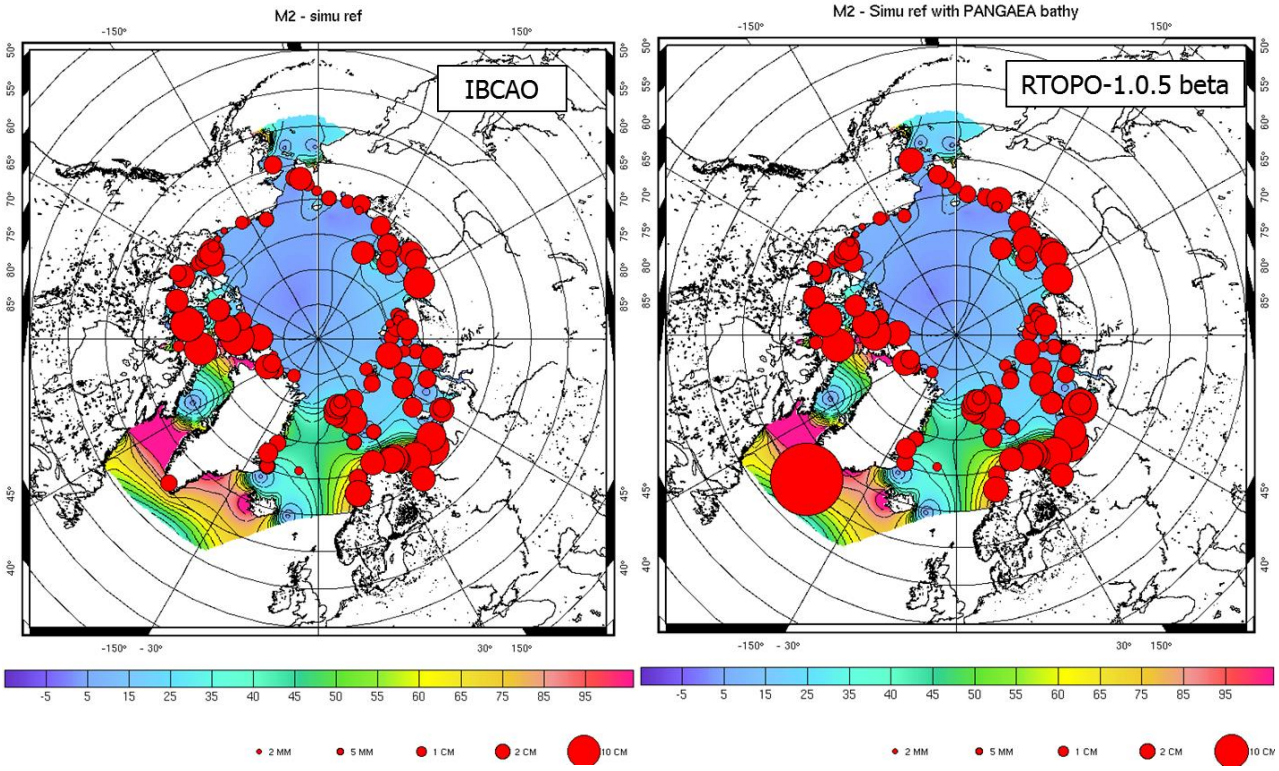

Figure 10: Hydrodynamic model performances for the M2 tidal component, using either the IBCAO bathymetry (left) or the R-Topo-1.0.5 beta bathymetry (right). The colors show the M2 amplitude (in cm) and the red dots show the vector differences compared to tide gauges.

Figure 11 shows each of these bathymetry datasets over Greenland. The scale was saturated in order to highlight some specific differences that clearly appears in Figure 12. For example, some large differences of more than 200 m are visible near the south-western coast of Greenland (encircled on each figure) and could explain the different results obtained with the hydrodynamic modelling.

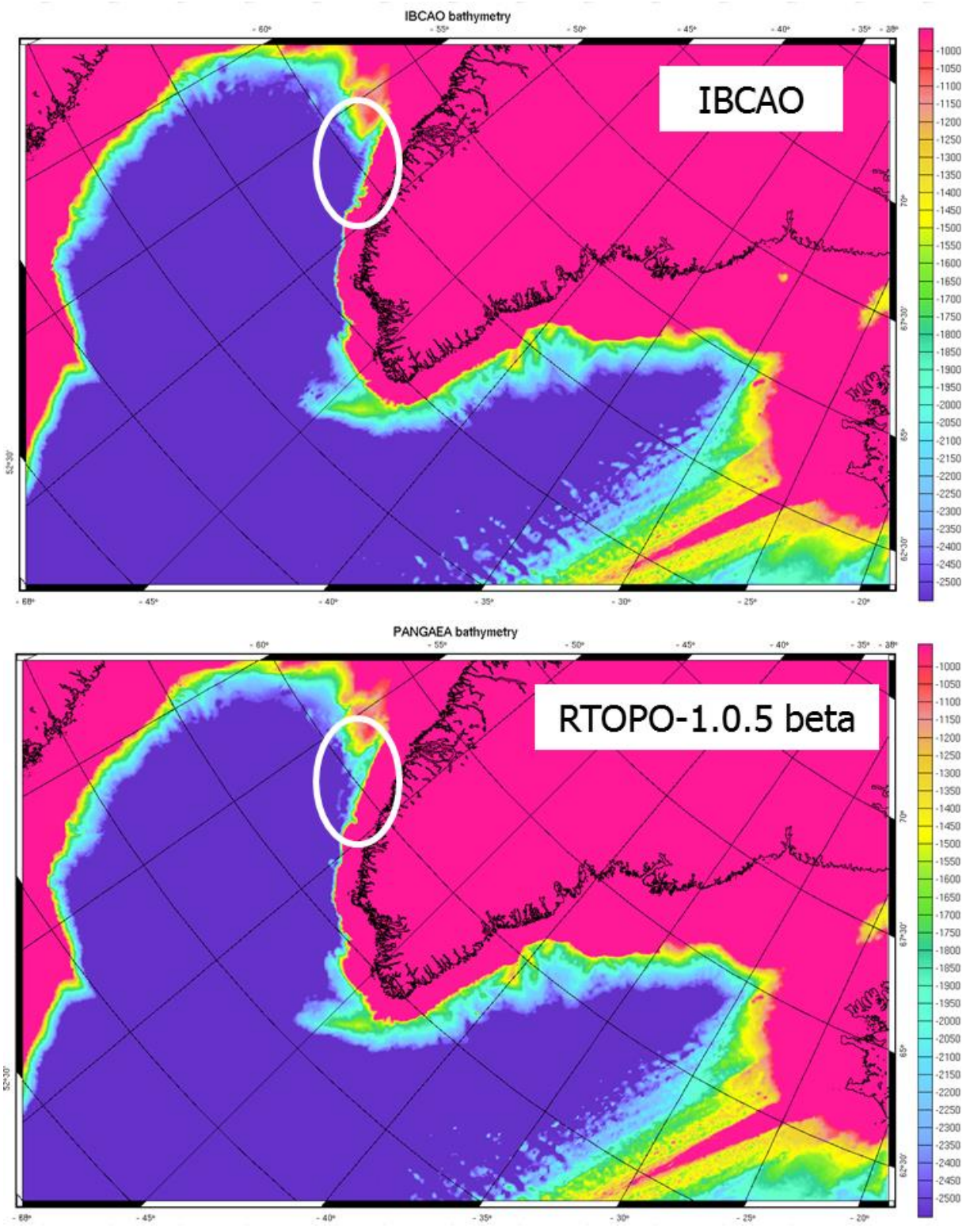

Figure 11: Zoom on the IBCAO (upper plot) and the R-Topo-1.0.5 beta (lower plot) bathymetry datasets over Greenland (in m).

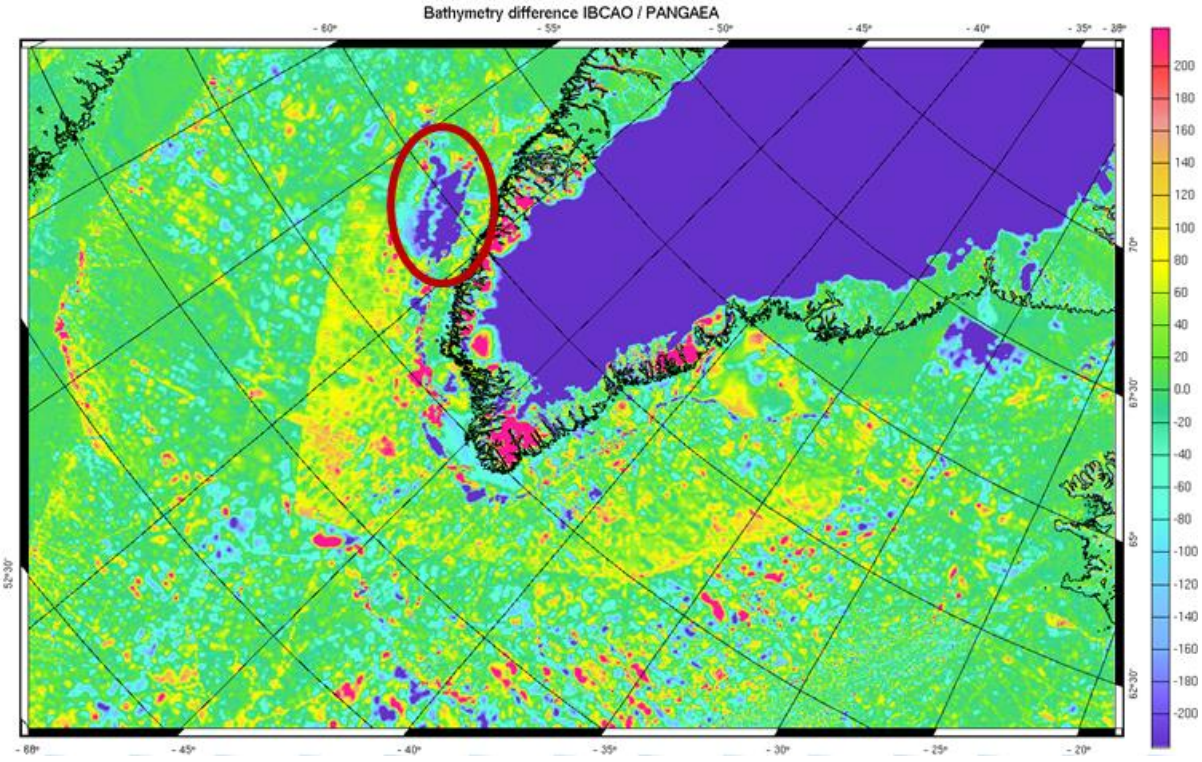

Figure 12: Difference (in m) between the IBCAO and the R-Topo-1.0.5 beta bathymetry datasets over Greenland.

This analysis confirmed the choice of the IBCAO bathymetry for this study. However, it also highlighted some differences between the two datasets that showed some defaults in the IBCAO bathymetry (with a smaller impact on the hydrodynamic simulation), such as some patches of high resolution data without any smoothing at the boundaries of the patches. In addition, a new version of the R-Topo bathymetry (R-Topo-2, [RD21]) was released very recently (but too late to be taken into account during this very study) with improvements around Greenland and it would be worth testing it in a later study.

2.3.5. Hydrodynamic model set-up and validation

The hydrodynamic model parameters need to be set up in order to obtain the reference hydrodynamic solution (see Figure 2).

The tidal boundary conditions used to run the regional hydrodynamic model in the Arctic Ocean are extracted from the FES2014 global model. At the coast, the boundaries are closed (no flow). At the open boundaries (ocean), the boundary conditions are applied to the tidal elevations (Dirichlet). The Neuman boundary conditions are known to be poorly efficient for tidal modelling, in particular in the case of a model formulated in wave equations, such as T-UGOm (F. Lyard, personal communication).

Some parameters of the T-UGOm hydrodynamic model need to be tuned in order to obtain the most accurate hydrodynamic solution. Generally, the two parameters to which the model is the most sensitive are:

- The bottom friction coefficient;
- The coefficient characterizing the energy transfer from the baroclinic mode to the barotropic mode, also called the wave drag coefficient.

The bottom friction dissipation is generally confined to some limited shelf regions, whereas the wave drag dissipation is widely spread in the ocean and can be the dominant dissipation mechanism in basins where the continental shelves are of relatively small extent [RD3].

The model set-up consists in varying each of these parameters separately in a large range of values in order to find the combination of parameters that gives the best solution. The parameters are varied around classical mean values, in an iterative process.

As the model is generally more sensitive to the bottom friction, it is the first parameter to be tuned. Then, the wave drag value is tested. Figure 13 shows the sensitivity of the T-UGOm hydrodynamic model to the bottom friction, for the four main tidal components in the Arctic Ocean (M2, S2, K1 and O1). The chosen formulation for the bottom friction coefficient C_D depends on the depth and the roughness length *Z0*. In particular, using low values of bottom friction coefficient clearly increases the error of the model, as shown by the vector differences to the tide gauge stations. Figure 14 shows that, on the contrary, the model is not sensitive to the wave drag coefficient value in this high-latitude region.

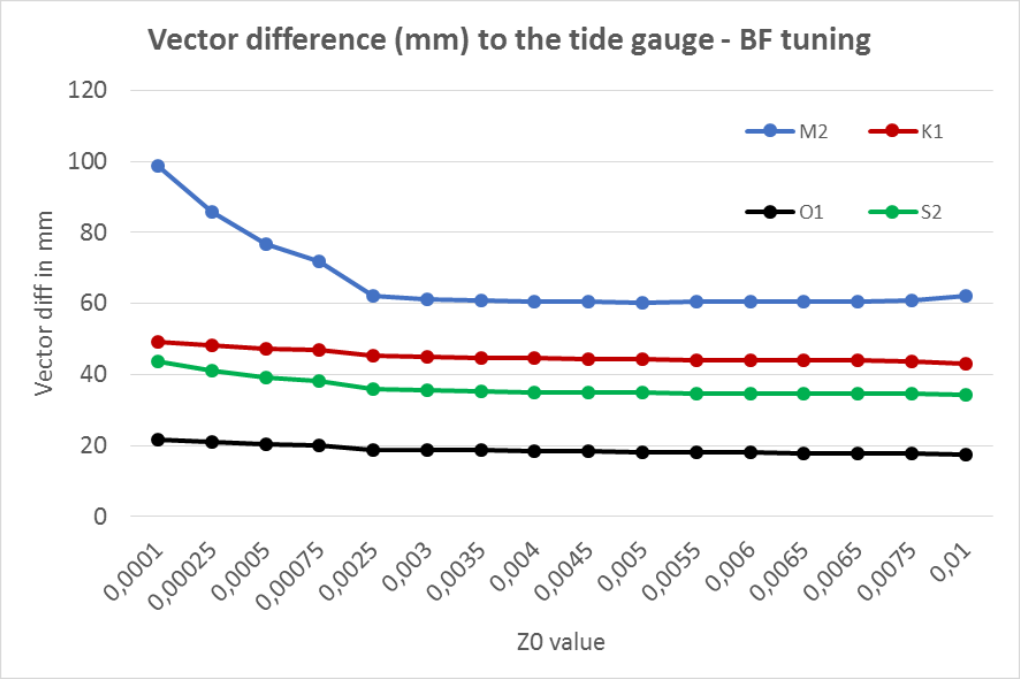

Figure 13: Vector difference between the hydrodynamic model and the tide gauge stations for the main tidal components (M2, S2, K1 and O1), for each hydrodynamic simulation performed in order to tune the bottom friction coefficient (roughness length Z0).

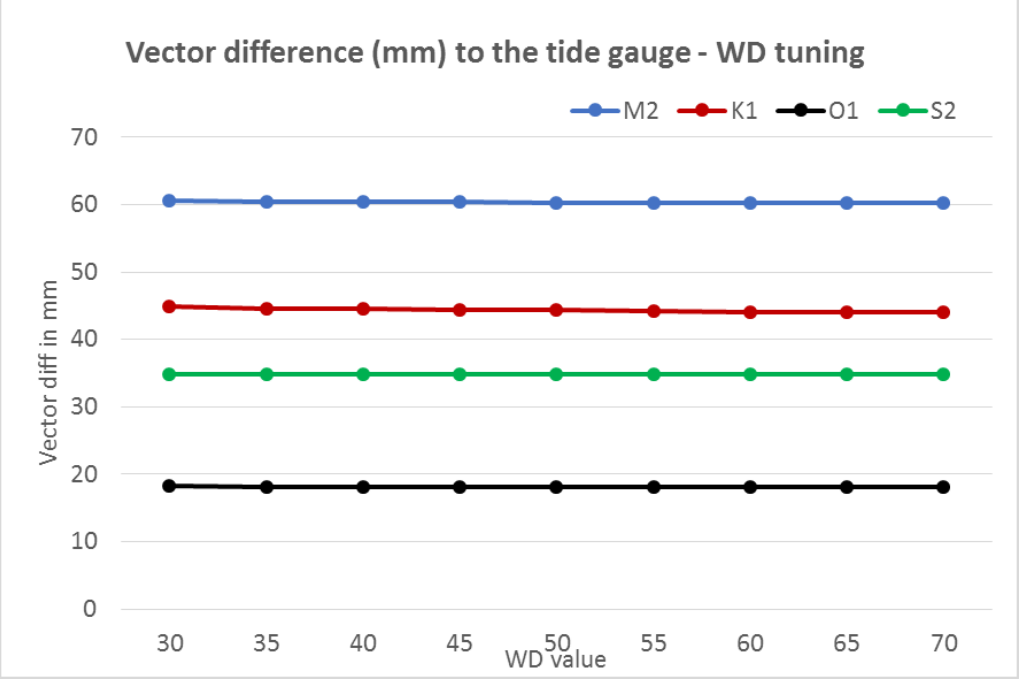

Figure 14: Vector difference between the hydrodynamic model and the tide gauge stations for the main tidal components (M2, S2, K1 and O1), for each hydrodynamic simulation performed in order to tune the wave drag coefficient (WD).

The values of parameters that were selected after this tuning exercise are as follows:

- Bottom friction coefficient: 0.005 m
- Wave drag coefficient: 50

The performances of the regional hydrodynamic simulation resulting from this parameter tuning are illustrated in Figure 15 (“ARCTIC” column). The performances of all the recent assimilated global models are also shown on the plot, as well as the results for the hydrodynamic simulation (no data assimilation) used for the computation of the FES2014 global model (“FES2014 hydro” column). The comparison to the tide gauge database (121 stations) shows that the regional hydrodynamic simulation performs equally or even better than the assimilated global models for the semi-diurnal components (M2 and S2), as it is highlighted by the red horizontal line that marks the performance of the regional model. This is due to two main reasons: the high resolution of the mesh and the boundary conditions extracted from the FES2014 global model.

For the diurnal tidal components (K1 and O1), the performances of the regional hydrodynamic model are still good, but the FES2014 global model (“FES2014” column) performs better, in particular for K1. This result could be linked to some physics regarding the wave drag definition at high latitude in the T-UGOm model. Indeed, the critical latitudes of the diurnal tidal components are far below 60° and the physics in the model might be different from reality at the scales reached by the regional model resolution. This effect is certainly smoothed in the FES2014 global model due to its larger grid, which explains the better performances of the global model for these tidal components. Improving these results would demand some developments and changes in the physics of the T-UGOm model that are far beyond the scope of this study. In addition, data assimilation is a way to constrain the tidal solution and obtain better performances, as it is shown in the following sections.

Finally, it should be noticed that the sea ice cover was not considered when tuning the parameters to obtain the best regional hydrodynamic solution. However, the results in section 2.4 show that the hydrodynamic model is also sensitive to this parameter. The sea ice cover seasonality was not accounted for in any of the global models as well, but it is likely that these global tidal models are closer to the “sea ice free” configuration, as the tide gauge and altimetry observations used for data assimilation or for optimal interpolation were mainly measured in sea ice free conditions.

Globally, the regional hydrodynamic non-assimilated solution (referred to as hydrodynamic prior solution in Figure 2) is of good quality and performs very well compared to the assimilated global models.

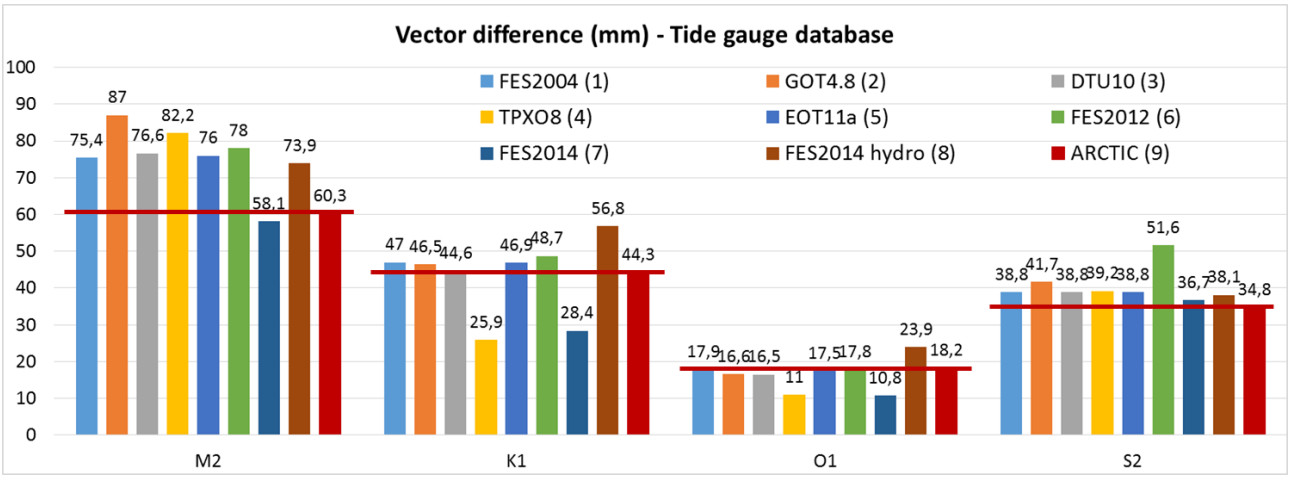

Figure 15: Performances of the hydrodynamic regional model in the Arctic Ocean (no data assimilation) and the global models, compared to the tide gauge observations, for the main tidal components. The red horizontal line marks the performance of the Arctic regional model.

2.4. Ensemble of simulations

The data assimilation method used for this project requires the covariance matrix of the errors of the prior hydrodynamic solution. The parameters computed with a numerical model such as T-UGOm (tidal elevations) contain errors for several reasons:

- The physics is not perfect in the model: the parameters that characterize some of the ocean dynamics processes are not well-known, which leads to the value of some parameters for some processes being approximated, or even neglected. For example, the local variations of the bottom friction coefficient are badly known. The definition of the wave drag coefficient that characterizes the energy transfer from the baroclinic mode to the barotropic mode also raises questions in some cases, as it was shown in the previous section, regarding the diurnal tidal components at high latitudes.
- The environmental data used as inputs in the model contain errors (bathymetry, coastline).
- The boundary conditions are not totally reliable, as they come from another model with a lower resolution.

A way to limit these sources of errors in the model consists in varying the parameters that drive these errors, thus generating an ensemble of perturbed simulations (generally about 20-30 simulations per parameter) centered on the prior hydrodynamic simulation obtained in section 2.3.5. The dispersion of this ensemble of simulations gives an estimate of the covariance matrix of the errors of the prior hydrodynamic solution, for each tidal component (see Figure 2).

In order to be sure that the perturbed simulations are realistic, each of them is validated against the tide gauge and the altimetry databases.

In the case of the Arctic Ocean, it was previously shown that the parameter that mainly drives the mode errors is the bottom friction coefficient. The wave drag coefficient, as currently defined in T-UGOm, has no strong impact on the hydrodynamic simulations in this region.

Regarding the bathymetry, the strategy is generally to compute hydrodynamic simulations with different bathymetry datasets. This is possible in the case of a global model, as there are different versions of the bathymetry products, with improvements in various regions of the globe. However in the case of the Arctic Ocean, the number of different datasets is too low to build an ensemble of perturbed simulations that would be representative of the model sensitivity to this parameter.

Consequently, the perturbed simulations were only performed on the bottom friction coefficient for this project. The analysis of the hydrodynamic model errors due to the bottom friction was done by dividing the model into sub-basins. In each of these zones, the bottom friction coefficient was varied in a range of values that are rather standard in the ocean. Figure 16 shows the partition of the regional model, based on the rate of energy dissipated because of the bottom friction. The sub-basins where the bottom friction coefficient has been varied are the areas of highest dissipation (red polygons). For each of these 8 polygons, 13 values of bottom friction coefficients were used for the hydrodynamic simulations: 0.0001; 0.0005; 0.001; 0.0025; 0.0075; 0.01; 0.015; 0.02; 0.025; 0.03; 0.04; 0.05; 0.1. This led to an ensemble of 104 simulations.

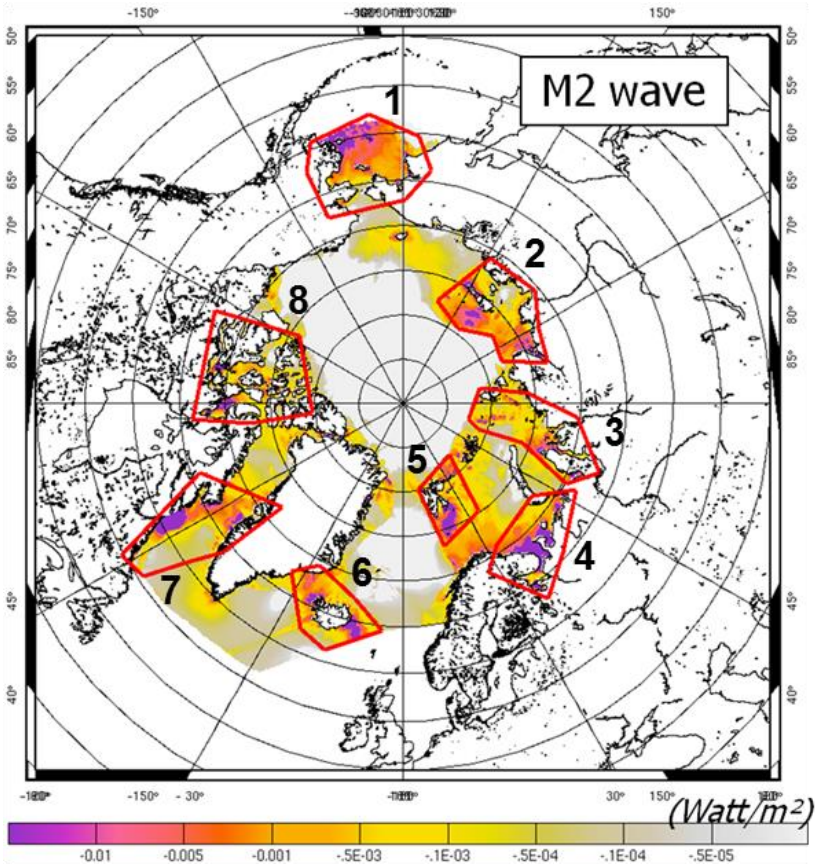

Figure 16: Energy dissipation due to the bottom friction for the prior hydrodynamic solution (M2 tidal component). The red polygons show the zones where the bottom friction coefficient has been varied to build the ensemble of simulations.

However, one of the important processes in the Arctic Ocean is the presence of sea ice, with strong seasonal variations. All the hydrodynamic simulations performed previously (including for the tuning of the model) considered neither ice shelf nor sea ice cover in the region. Figure 17 shows the sea ice extent in winter (on the left) and in summer (on the right) during the year 2014. The maps are provided by the NSIDC (National Snow and Ice Data Center) in Colorado (USA). The pink line on each plot shows the median sea ice extent computed over 30 years.

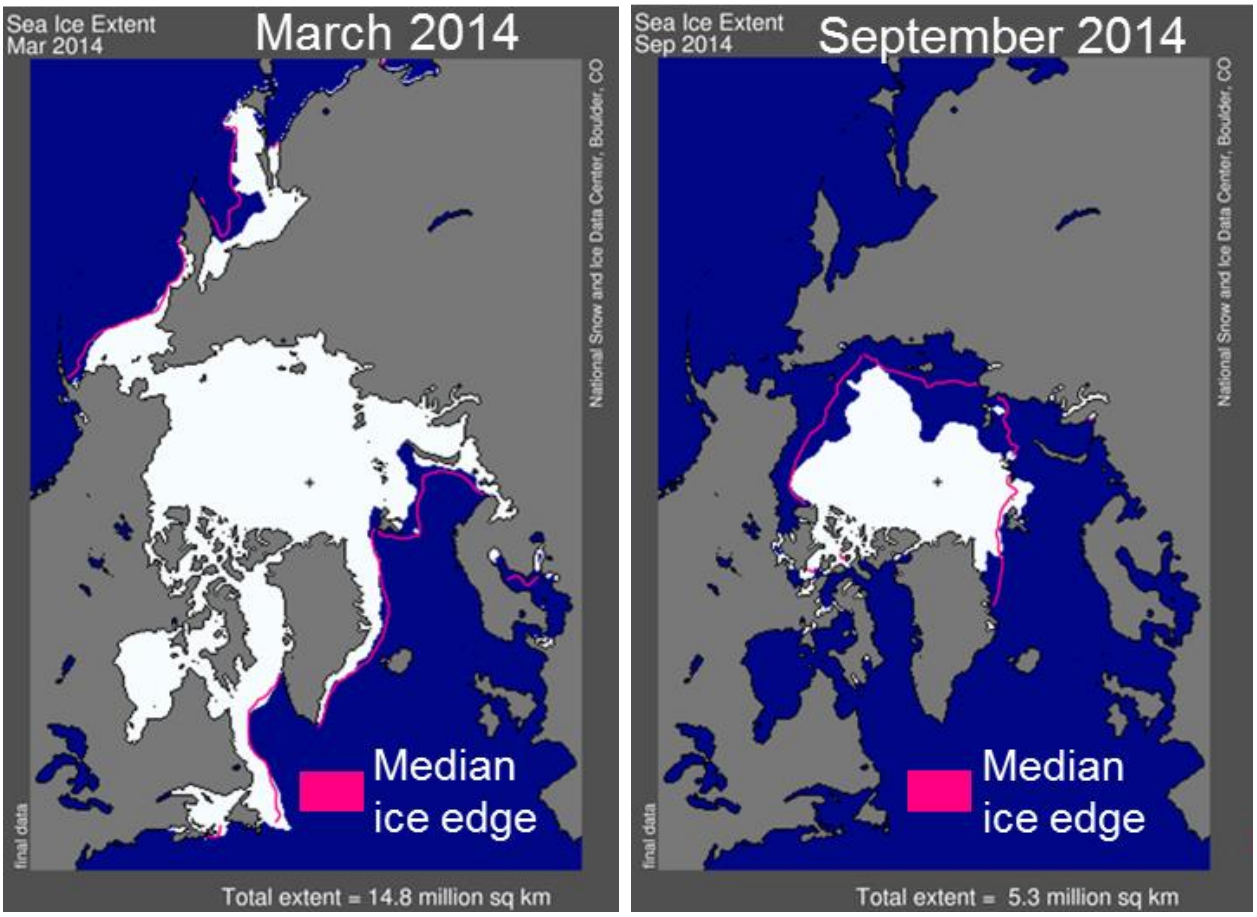

Figure 17: Sea ice extent in March 2014 (left) and September 2014 (right) and median ice edge computed over 30 months of March (left) and September (right), from 1981 to 2010. Maps from the NSIDC.

Considering that the friction in the T-UGOm model not only happens at the bottom but also under the sea ice cover, at the sea surface, the sea ice cover was introduced in the model as polygons where the dissipation due to the friction is multiplied by a factor of two (friction at the bottom and friction at the surface). The factor of two is almost arbitrary chosen as it should depend on the type and roughness of the sea ice, but this is a first approximation.

Two configurations were defined:

- winter configuration, based on the median extent of the month of March;
- summer configuration, based on the median extent of the month of September.

The extent polygons were drawn using the shapefiles provided by NSIDC with this information, and introduced in the model. All the simulations with the local variations of the bottom friction coefficient were re-run twice, using the sea ice cover information. The final ensemble of perturbed simulations is consequently composed of 312 hydrodynamic simulations.

Figure 18 to Figure 21 show the vector differences between all the perturbed hydrodynamic simulations and the altimetry data, for M2, S2, K1 and O1 respectively. The simulations are gathered by polygon (see Figure 16) and from the lowest to the highest values of bottom friction coefficient. Figure 22 to Figure 25 show the same diagnostics for the tide gauge database.

The colours show the different sea ice extents:

- Base: no sea ice at all;
- Ice extent March: winter configuration;
- Ice extent Sept: summer configuration.

The largest variations in the results are observed for the tidal components with the largest amplitudes in the area (M2 and K1). There is no unrealistic simulation (no large difference from one simulation to the next) and some regions appear to provide more variability than the others, depending on the diurnal or semi-diurnal type of the tidal component, which is what was expected. For example, the M2 semi-diurnal tidal component shows more variability in the polygons 4 (Barents Sea) and 5 (Svalbard) whereas the K1 diurnal tidal component is more sensitive to the bottom friction coefficient in the polygon 8 (North-West Passage).

These results are consistent with the fact that the largest amplitudes for K1 are observed in the Baffin Sea (polygon 7) and in the North-West Passage (polygon 8). For M2, the largest amplitudes are located in the Southern part of Greenland and along the Scandinavian coasts up to the Barents Sea (polygon 4).

It is also interesting to note the impact of the sea ice cover. For the K1 diurnal tidal component, the vector differences to both the altimetry and the tide gauge datasets are reduced when considering the winter configuration for the sea ice extent (March). On the contrary, the M2 semi-diurnal tidal component is closer to the observations when the smallest sea ice extent is considered and the results are very close for the summer case and the case without any sea ice cover at all.

Finally, it can be noticed that the vector differences are generally higher when comparing to the tide gauge dataset than when comparing to the altimetry dataset. The tide gauge stations are often located in sheltered regions and fjords that are not representative of the open ocean tide, contrary to the altimetry data. In addition, there may be some seasonal artefacts in the comparisons, due to the fact that more tide gauge and altimetry measurements are available in summertime, when there is less sea ice. However, we do not have the tide gauge SSH time series and we do not know when the tide gauge measurements were made.

In prevision of data assimilation, all the 312 perturbed simulations have been computed for the 8 tidal components available in the altimetry-derived harmonic constituents provided by DTU Space: M2, S2, K1, O1, K2, N2, P1 and Q1.

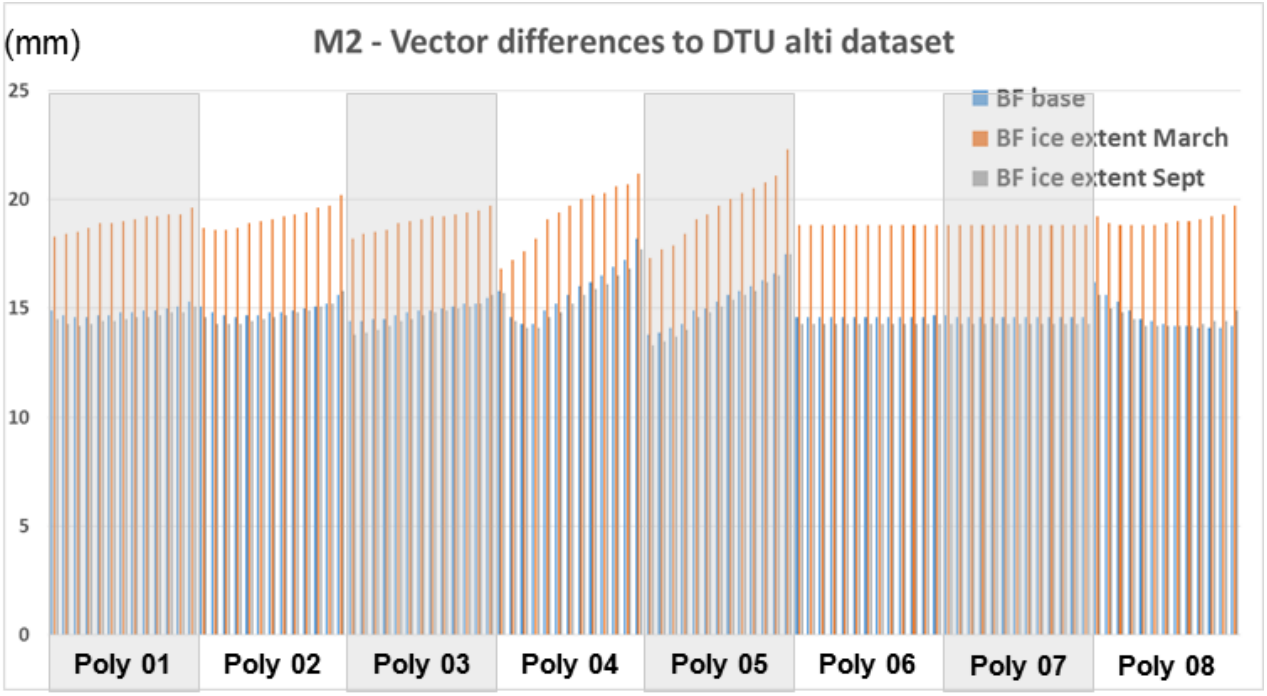

Figure 18: Vector differences between the altimetry data and each of the perturbed simulations of the bottom friction coefficient ensemble. The numbers of the polygons refer to Figure 16. M2 tidal component.

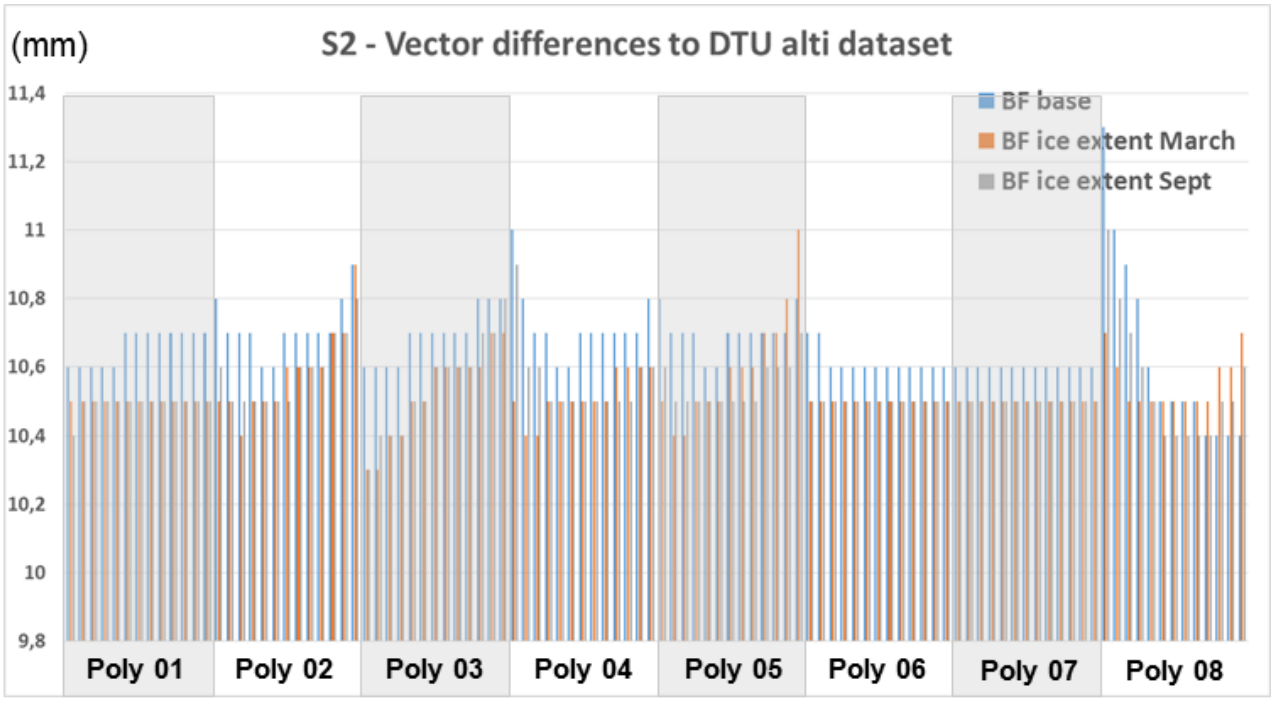

Figure 19 : Vector differences between the altimetry data and each of the perturbed simulations of the bottom friction coefficient ensemble. The numbers of the polygons refer to Figure 16. S2 tidal component.

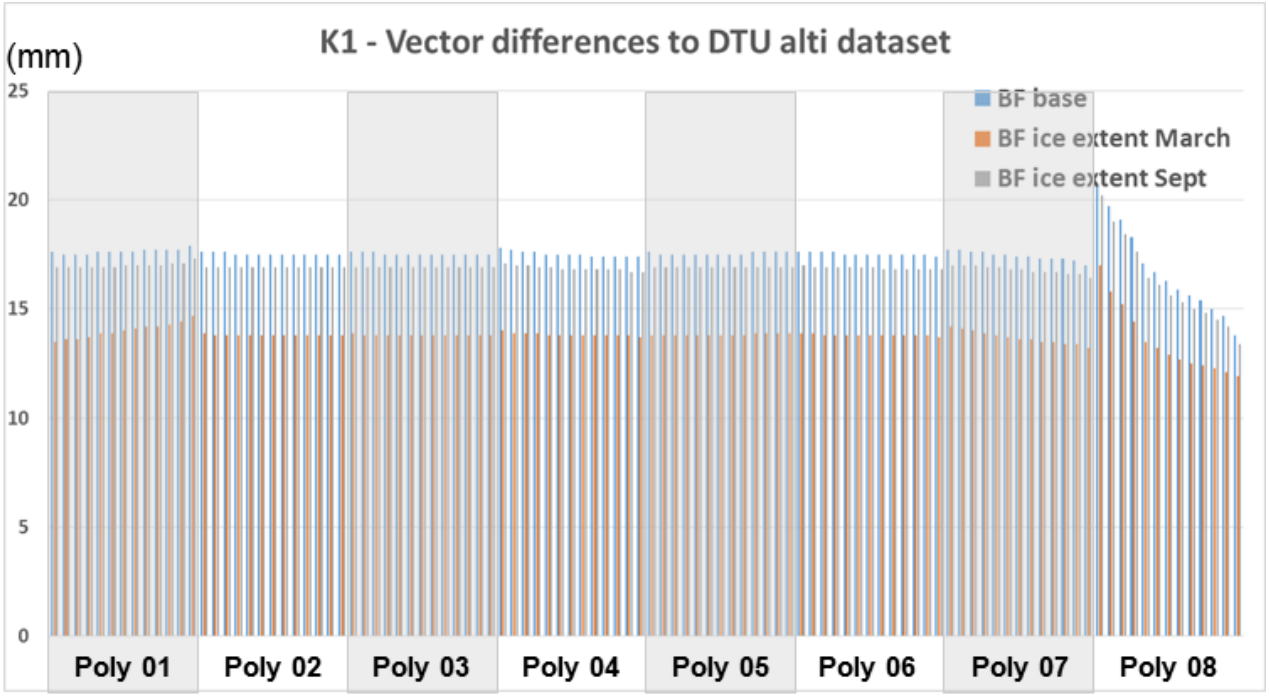

Figure 20: Vector differences between the altimetry data and each of the perturbed simulations of the bottom friction coefficient ensemble. The numbers of the polygons refer to Figure 16. K1 tidal component.

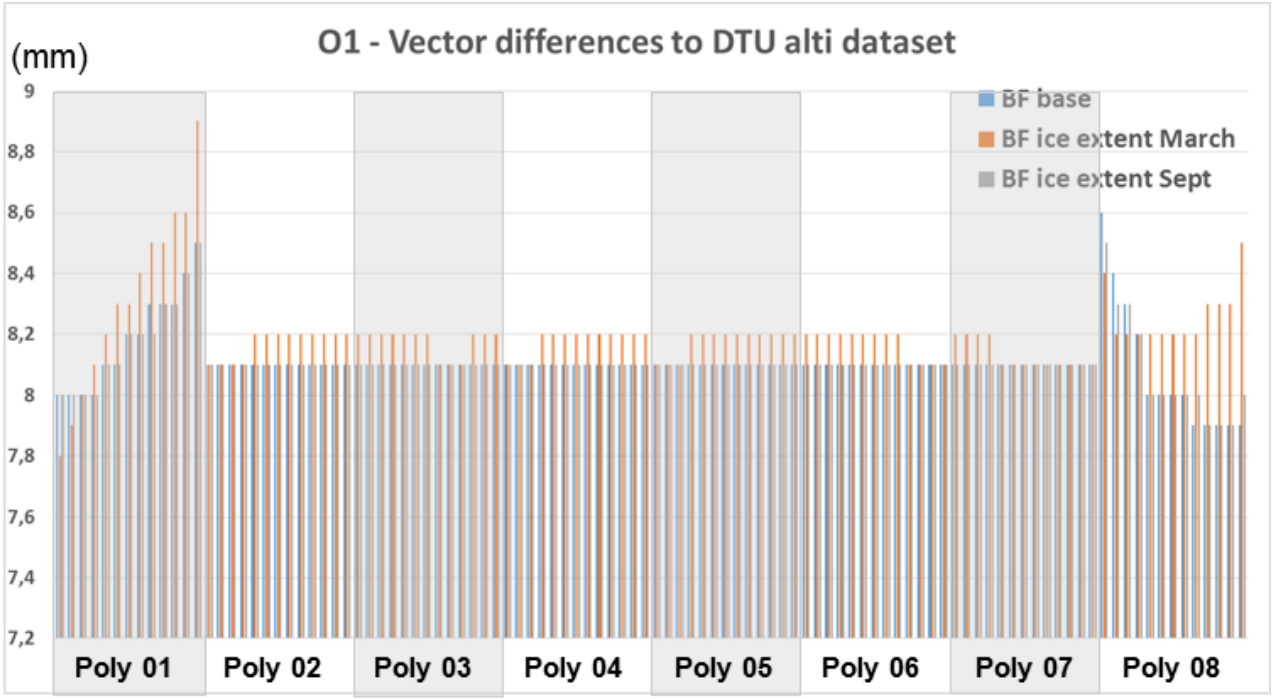

Figure 21: Vector differences between the altimetry data and each of the perturbed simulations of the bottom friction coefficient ensemble. The numbers of the polygons refer to Figure 16. O1 tidal component.

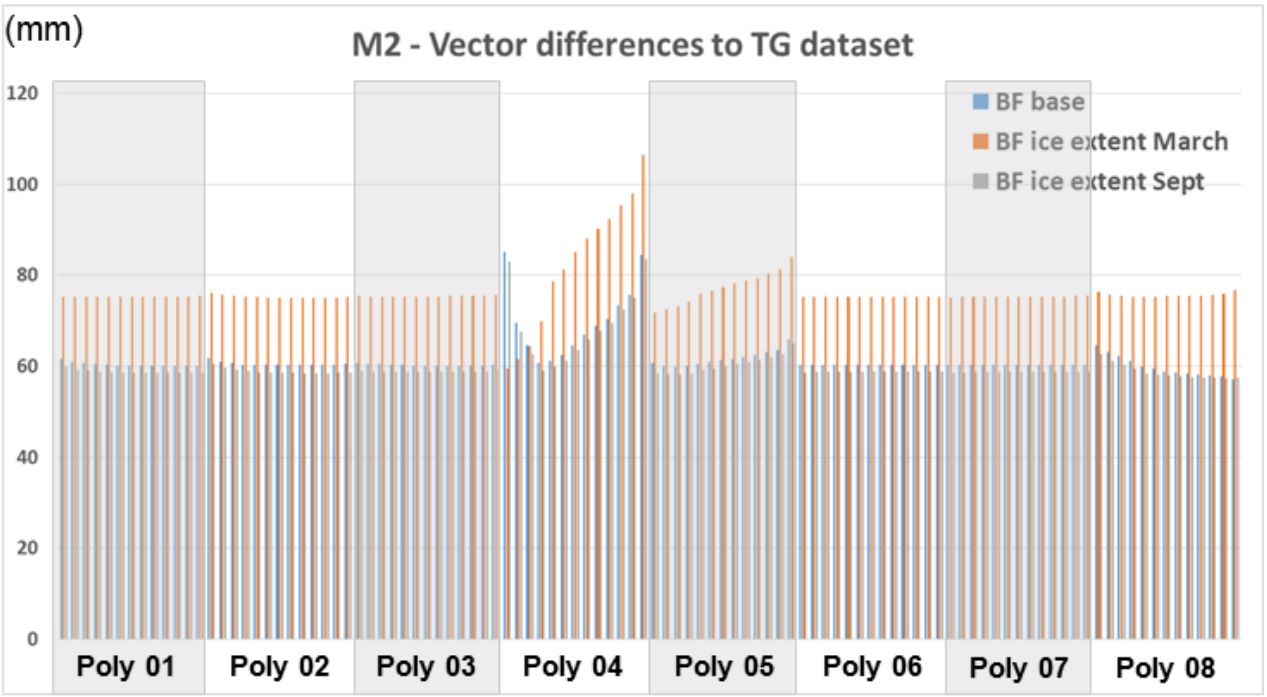

Figure 22: Vector differences between the tide gauge data and each of the perturbed simulations of the bottom friction coefficient ensemble. The numbers of the polygons refer to Figure 16. M2 tidal component.

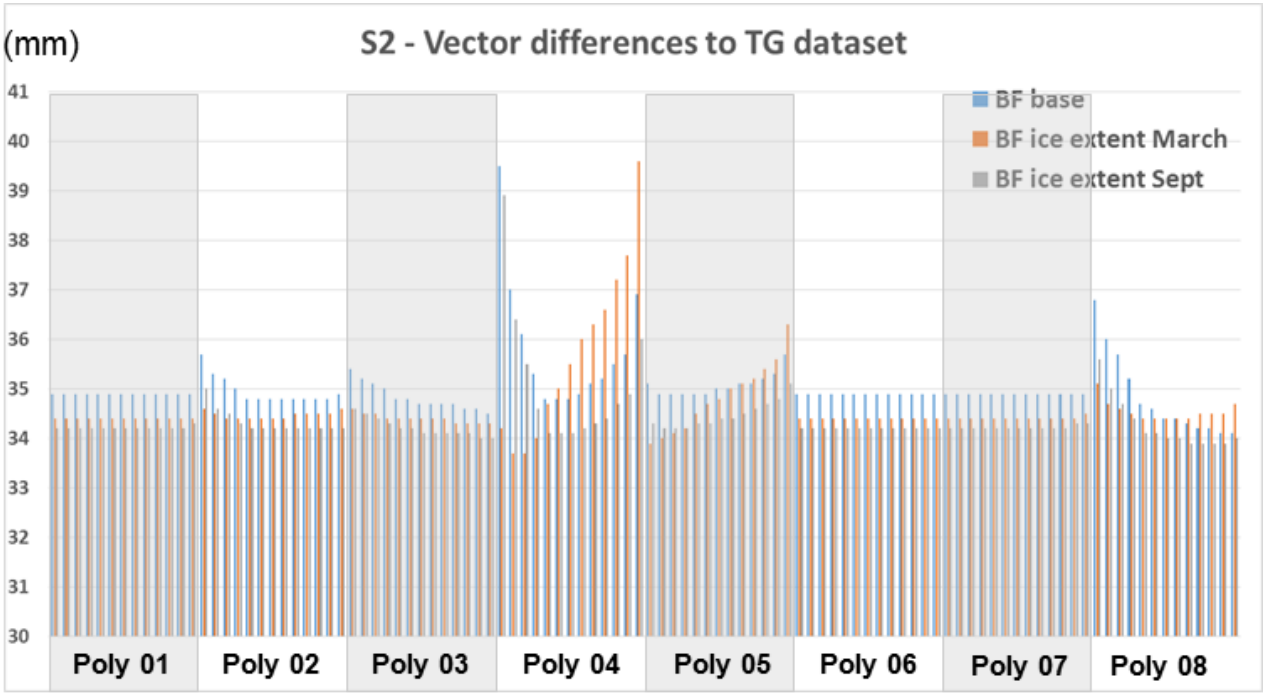

Figure 23: Vector differences between the tide gauge data and each of the perturbed simulations of the bottom friction coefficient ensemble. The numbers of the polygons refer to Figure 16. S2 tidal component.

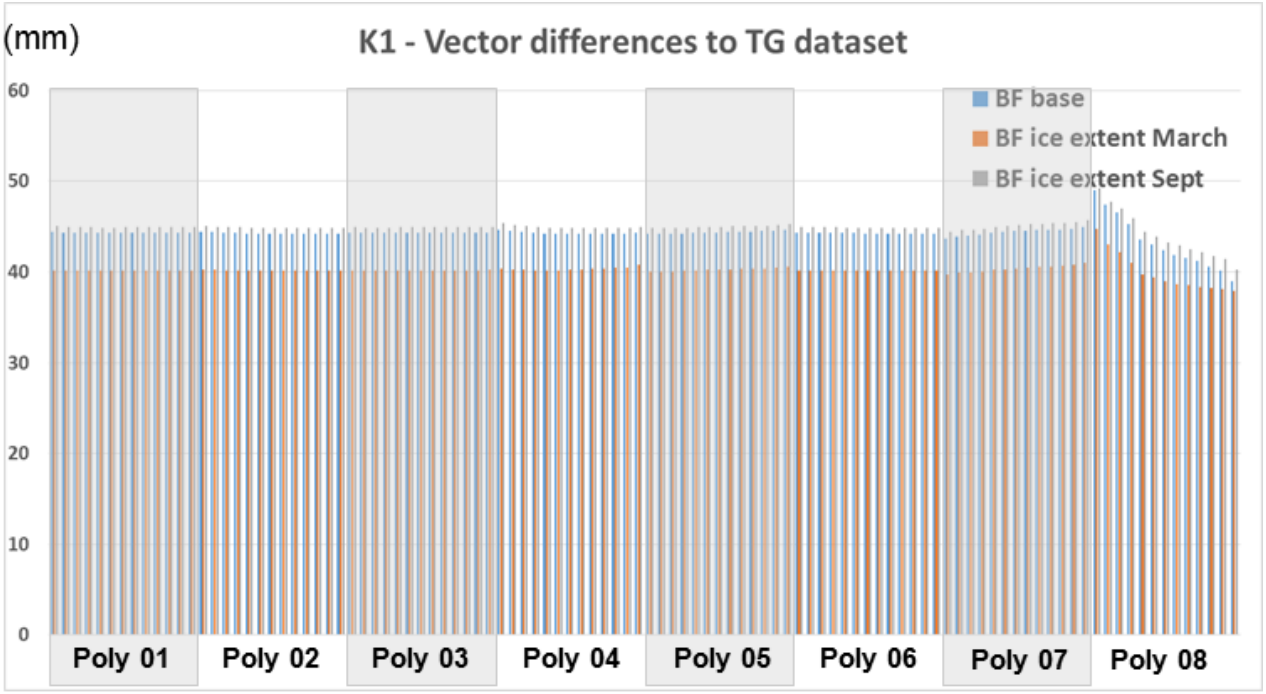

Figure 24: Vector differences between the tide gauge data and each of the perturbed simulations of the bottom friction coefficient ensemble. The numbers of the polygons refer to Figure 16. K1 tidal component.

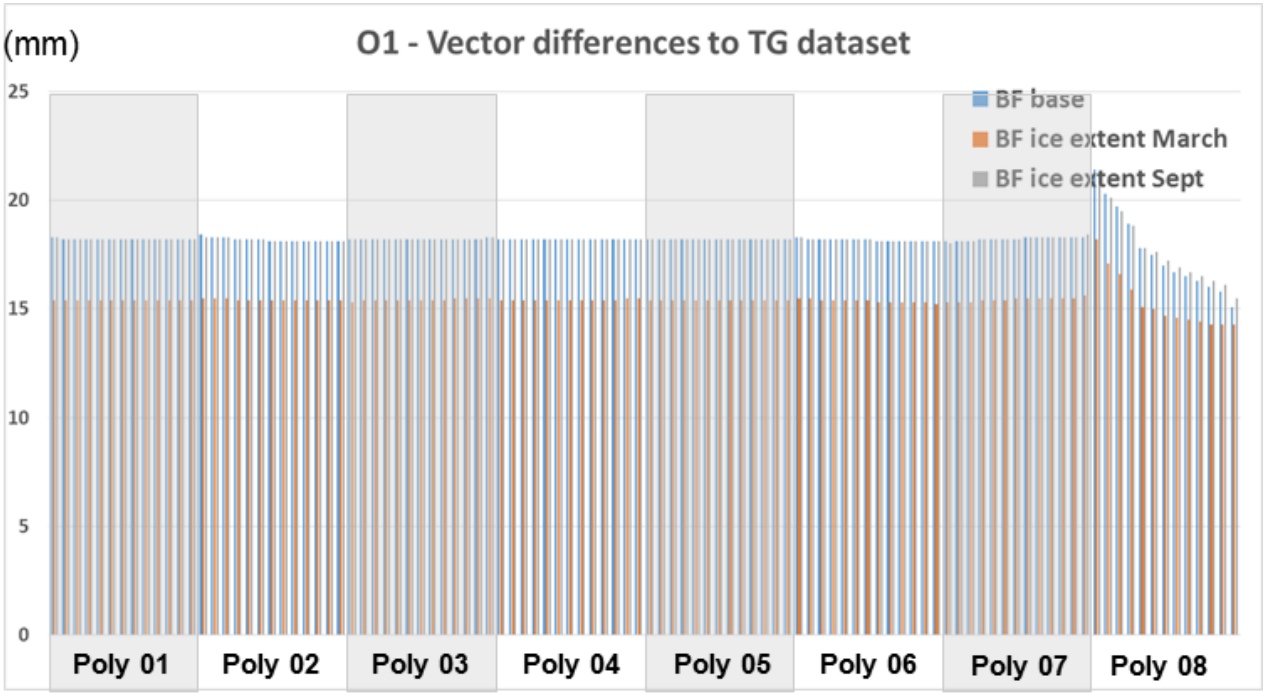

Figure 25: Vector differences between the tide gauge data and each of the perturbed simulations of the bottom friction coefficient ensemble. The numbers of the polygons refer to Figure 16. O1 tidal component.

2.5. Data assimilation

2.5.1. Methodology

The aim of this part of the project is to improve the prior hydrodynamic solution by assimilating altimetry and tide gauge observations (Figure 2). The objective is to generate data assimilated solutions that minimize the distance between the prior non-assimilated hydrodynamic simulation and the observations, taking into account their respective errors. The assimilated solutions are thus **optimal** in the least squares sense as they are coherent with both the observations and the physical structures described by the T-UGOm hydrodynamic model.

The assimilation method is based on the ensemble Kalman Filter in a formulation based on the notion of representer functions for the observations (Bennett, 1992, [RD22] ; Lyard, 1997, [RD23] ; Echevin *et al.*, 2000, [RD24] ; Evensen, 2003 [RD25]). In this very study, the assimilation is not performed in time-stepping as the objective is to correct the tidal harmonic constituents from the hydrodynamic model with tidal harmonic constituents derived from the harmonic analysis of altimetry and tide gauge sea surface height time series. The problem can be formulated as follows:

$$\mathbf{x}^a = \mathbf{x}^f + \mathbf{P}^f \mathbf{H}^T \left(\mathbf{H}\mathbf{P}^f \mathbf{H}^T + \mathbf{R}\right)^{-1} \left(\mathbf{y}^o - \mathbf{H}\mathbf{x}^f\right) \qquad \text{(eq.2)}$$

$$= \mathbf{x}^f + \sum_{n=1}^{p} \mathbf{r}_n \mathbf{b}_n \qquad \text{(eq.3)}$$

$$= \mathbf{x}^f + \mathbf{r}\mathbf{b} \qquad \text{(eq.4)}$$

where:

$\mathbf{x}^a$ is the field of a given tidal harmonic constituent after the assimilation process (analyzed state vector);

$\mathbf{x}^f$ is the field of the same tidal harmonic constituent before the assimilation process (estimated state vector);

$\mathbf{P}^f$ is the covariance matrix of the model errors;

$\mathbf{R}$ is the covariance matrix of the observations errors;

$\mathbf{H}^T$ is the observation operator that ensures the projection from the model space to the observations space;

$\mathbf{Y}^0$ is the observation;

$\mathbf{r}_n$ is the representer of the n observation;

$\mathbf{b}_n$ is a coefficient vector associated with $\mathbf{r}_n$;

P is the number of observations.

Given (eq.2) and (eq.4), the matrices $\mathbf{r}$ and $\mathbf{b}$ are defined by the following relations:

$$\mathbf{r} = \mathbf{P}^f \mathbf{H}^T \qquad \text{(eq.5)}$$

$$\left(\mathbf{H}\mathbf{P}^f \mathbf{H}^T + \mathbf{R}\right)\mathbf{b} = \left(\mathbf{y}^o - \mathbf{H}\mathbf{x}^f\right) \qquad \text{(eq.6)}$$

The number of columns of the $\mathbf{r}$ matrix is the number of observations and the $\mathbf{r}_n$ column is the representer of the n observation. The representer analysis (eq.2) can be seen as the correction of the estimated state $\mathbf{x}^f$ with a combination of terms – the representers – that depend on the covariance matrix of the model errors ($\mathbf{P}^f$). Each representer $\mathbf{r}_n$ thus propagates the information of the n observation to the various variables of the model that are taken into account in the state vector. The representers consequently define the *influence domain* of the observations.

With this approach, the covariances of the model errors are estimated through **ensemble stochastic modelling**. An ensemble of model simulations is generated with perturbations of one or more parameters of the model.

In the case of the Arctic tidal atlas, the model parameter that was perturbed to generate the ensemble is the bottom friction coefficient, with various sea ice cover conditions as explain in section 2.4 of this report.

The covariances of the model errors can be estimated by the **ensemble covariances of the model errors**.

In the frame of the hypotheses of BLUE (Best Linear Unbiased Estimator) and stochastic modelling, the errors of the model are supposed to be unbiased, i.e. zero-mean. As a consequence, the **ensemble covariances of the model errors** can be identified to the **ensemble covariances of the model variables:**

$$\mathrm{cov}\left(\boldsymbol{\varepsilon}_k^f, \boldsymbol{\varepsilon}_i^f\right) = \frac{1}{N}\sum_{j=1}^{N}\left(\varepsilon_{k,j}^f - \frac{1}{N}\sum_{j=1}^{N}\varepsilon_{k,j}^f\right)\left(\varepsilon_{i,j}^f - \frac{1}{N}\sum_{j=1}^{N}\varepsilon_{i,j}^f\right) \qquad \text{(eq.7)}$$

$$= \frac{1}{N}\sum_{j=1}^{N}\left(\varepsilon_{k,j}^f\right)\left(\varepsilon_{i,j}^f\right) \qquad \text{(eq.8)}$$

$$= \frac{1}{N}\sum_{j=1}^{N}\left(x_{k,j}^f - \frac{1}{N}\sum_{j=1}^{N}x_{k,j}^f\right)\left(x_{i,j}^f - \frac{1}{N}\sum_{j=1}^{N}x_{i,j}^f\right) \qquad \text{(eq.9)}$$

$$= \mathrm{cov}\left(\mathbf{x}_k^f, \mathbf{x}_i^f\right) \qquad \text{(eq.10)}$$

where ε_k^f (respectively ε_i^f) is the estimate error of the x_k^f (respectively x_i^f) model variable at the *k* (respectively *i*) point of the domain, that can be formulated as:

$$\boldsymbol{\varepsilon}_k^f = \mathbf{x}_k^f - \frac{1}{N}\sum_{j=1}^{N}x_{k,j}^f \qquad \text{(eq.11)}$$

with *N* the dimension of the ensemble.

Then, the **influence domain** of a given observation can be explained as follows. If $\mathbf{y}_k$ is a given observation (complex observation defined by amplitude and phase lag) of the $\mathbf{x}_k$ variable (complex variable defined by amplitude and phase lag) located on the k node of the mesh (this to simplify the expressions, as the observation operator **H** can be expressed as the identity matrix and $\mathbf{y}_k$ is "equivalent" to $\mathbf{x}_k$ in this case), the correction applied to the estimated state $\mathbf{x}^f$ through the assimilation of the $\mathbf{y}_k$ observation can be written as follows:

$$\delta\mathbf{x} = \mathbf{x}^a - \mathbf{x}^f = \mathbf{b}_k\mathbf{r}_k \qquad \text{(eq.12)}$$

with :

$$\mathbf{r}_k = \mathbf{P}^f\mathbf{H}_k^T = \mathrm{cov}\left(\varepsilon_k^f, \varepsilon_i^f\right) \qquad \text{(eq.13)}$$

$$\mathbf{b}_k = \frac{\mathbf{y}_k - \mathbf{x}_k}{\mathrm{cov}\left(\varepsilon_k^f, \varepsilon_k^f\right) + \mathrm{cov}\left(\varepsilon^o, \varepsilon^o\right)} = \frac{\delta\mathbf{y}_k}{\mathrm{var}\left(\varepsilon_k^f\right) + \mathrm{var}\left(\varepsilon^o\right)} \qquad \text{(eq.14)}$$

where $\delta\mathbf{y}_k$ is the innovation (vector difference between the observation and the model), ε_k^f is the estimate error, ε^o is the observation error and « var » is the ensemble variance function.

By combining (eq.12), (eq.13) and (eq.14), the correction at node i is:

$$\delta\mathbf{x}_i = \frac{\mathrm{cov}\left(\varepsilon_k^f, \varepsilon_i^f\right)}{\mathrm{var}\left(\varepsilon_k^f\right) + \mathrm{var}\left(\varepsilon^o\right)}\delta\mathbf{y}_k \qquad \text{(eq.15)}$$

or, using the correlations of the errors:

$$\mathrm{correl}\left(\varepsilon_k^f, \varepsilon_i^f\right) = \frac{\mathrm{cov}\left(\varepsilon_k^f, \varepsilon_i^f\right)}{\sqrt{\mathrm{var}\left(\varepsilon_k^f\right)\mathrm{var}\left(\varepsilon_i^f\right)}} \qquad \text{(eq.16)}$$

$$\delta \mathbf{x}_i = \frac{\mathrm{correl}\left(\varepsilon_k^f, \varepsilon_i^f\right)}{1 + \frac{\mathrm{var}\left(\varepsilon^o\right)}{\mathrm{var}\left(\varepsilon_k^f\right)}} \sqrt{\frac{\mathrm{var}\left(\varepsilon_i^f\right)}{\mathrm{var}\left(\varepsilon_k^f\right)}}\, \delta \mathbf{y}_k \qquad \text{(eq.17)}$$

As a consequence, the correction obtained through the assimilation of a given observation $\mathbf{y}_k$ depends on the correlations between the errors associated with both the observed variable ($\mathbf{x}_k$) and the model variable to be corrected ($\mathbf{x}_i$). This highlights the spatial extension of the correction.

The amplitude of the correction $\delta \mathbf{x}_i$ depends on the observation error and the ratio between the error variances at the point i of the mesh and at the observation location. If the observation error is higher than the model error, there is no need to strongly constrain the model and the correction is weak. If the model error is higher than the observation error, it is the reverse. In addition, the amplitude of the correction $\delta \mathbf{x}_i$ is directly linked to the error variance of the model at point i compared to the observation location.

It is also possible to restrain the spatial influence of a given observation in the assimilation code by using a decorrelation function that comes to zero at a specific distance, defined as a function of the model domain and the size of the tidal structures in the region.

2.5.2. Data selection

The observations dataset used for the assimilation was carefully built in order to constrain the tidal hydrodynamic model with accurate data and generate the most accurate optimal tidal atlas.

2.5.2.1. Altimetry data

The altimetry-derived tidal harmonic constituents were computed by DTU Space with the method described in section 2.2. The altimetry tidal observations are available on a 1°x3° grid, which represents a total of 1745 points included in the Arctic regional model domain (Figure 26, left-hand plot). Eight linear tidal components were provided by DTU Space (M2, S2, K1, O1, N2, P1, Q1).

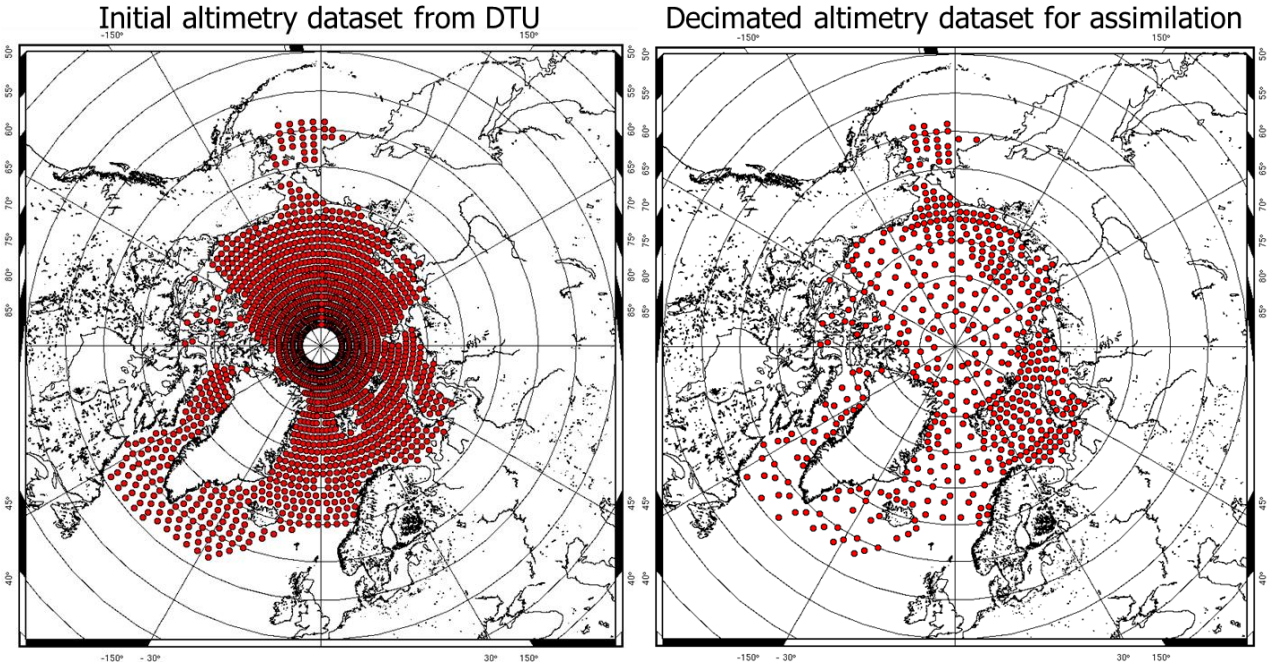

Figure 26: Initial (left, 1745 points) and decimated (right, 507 points) altimetry-derived tidal constituent dataset provided by DTU Space, selection over the Arctic tidal model domain.

Of course, the density of points increases highly close to the North Pole. On the other hand, the amplitude of the tide is very low close to the North Pole (see Figure 27), which means that the model errors are small in this region. There is no need to strongly constrain the model with a lot of observations that would not bring additional useful information in the data assimilation process. More importantly, given that the errors in the prior hydrodynamic solution are small and that the altimetry data are not perfect, the choice was made to maintain a balance between the weight of the observations and the weight of the model. This is why the altimetry dataset was decimated in the open ocean before the data assimilation. The selection was simply done by considering the distance between two points in the open ocean (200 km). On the shelves, all the altimetry data were kept in the selection. In the end, the altimetry-derived dataset has 507 points (Figure 26, right-hand plot), with a high density on the Siberian shelf and in the Bering Strait.

The same selection was performed for all the assimilated tidal components (M2, S2, K1, O1, N2, P1, Q1), except for the K2 tidal component. Indeed, for this particular tidal component, the validation of the various assimilation tests showed that the altimetry data tended to constrain the model in a different way compared to the tide gauges. The K2 tidal component is strongly aliased with the semi-annual signal at the Envisat repeat period [RD10], which makes it difficult to accurately separate this tidal component in the harmonic analysis of the altimetry sea surface height time series. Consequently, no altimetry data was assimilated in the K2 solution.

No error estimate was provided with the altimetry data. As the data assimilation process needs observation error estimates, as explained in section 2.5.1, a single arbitrary value was chosen for each tidal component, equivalent to about 5-10% of its maximum amplitude in the region (see Table 2). Of course, an error estimate evaluated at each point of the altimetry data grid during the tidal harmonic analysis process would have helped to discriminate possible dubious altimetry observations. With a fixed arbitrary value, all the altimetry observations have the same weight in the data assimilation process, whatever their quality.

Table 2: Error estimate values attributed to the altimetry-derived tidal constituents, for each tidal component.

Tidal component	**M2**	**S2**	**K1**	**O1**	**N2**	**P1**	**Q1**
Error estimate	2 cm	1 cm	1.5 cm	1 cm	1 cm	1 cm	1 cm

Another important point to keep in mind regarding this altimetry dataset is the fact that the annual signal was not totally removed from the altimetry sea surface height time series before the tidal harmonic analysis process, which means that the diurnal components (in particular K1 and P1) are not perfectly separated from this signal (see section 2.2.4).

2.5.2.2. Tide gauge data

As it was described in section 2.3.2, the tide gauge data available in the Arctic Ocean are scarce and sometimes dubious. Throughout this study, some stations were removed from the database of 121 tide gauge stations (already resulting from a long-term strict editing process), when identified as dubious. In particular, a selection was performed thanks to an assimilation test for the M2 tidal component. Only altimetry data were assimilated in this test, in order to obtain a tidal solution totally independent from the tide gauge database. Then, the vector differences between the tidal model and the tide gauges were computed (left-hand plot in Figure 27). All the tide gauges with large (>20 cm) misfits to the altimetry-only assimilated model were discarded, resulting in a reduced database which was used for the assimilation. Starting with 121 stations in the initial tide gauge dataset (before the assimilation test but after previous editing steps – the original tide gauge database had more than 500 stations), the final database contains 105 stations.

Unfortunately, for most of the tide gauge stations, the time series are not distributed and the number of tidal components is reduced to two or three components. The tidal constituents of all the available components were assimilated. In addition, as for the altimetry dataset, no error estimate was provided with the tide gauge data. An arbitrary value was also chosen for all the tide gauges, depending on the amplitude of the tidal components. The number of stations and the error estimate values for each tidal component are summarized in Table 3.

Table 3: Number of tide gauge stations in the assimilation dataset and error estimate values attributed to the tide-gauge-derived tidal constituents, for each tidal component.

Tidal component	M2	S2	K1	O1	K2	N2	P1	Q1
Number of tide gauge stations	105	100	96	94	51	61	52	36
Error estimate	2 cm	1 cm	1.5 cm	1 cm	1 cm	1 cm	1 cm	1 cm

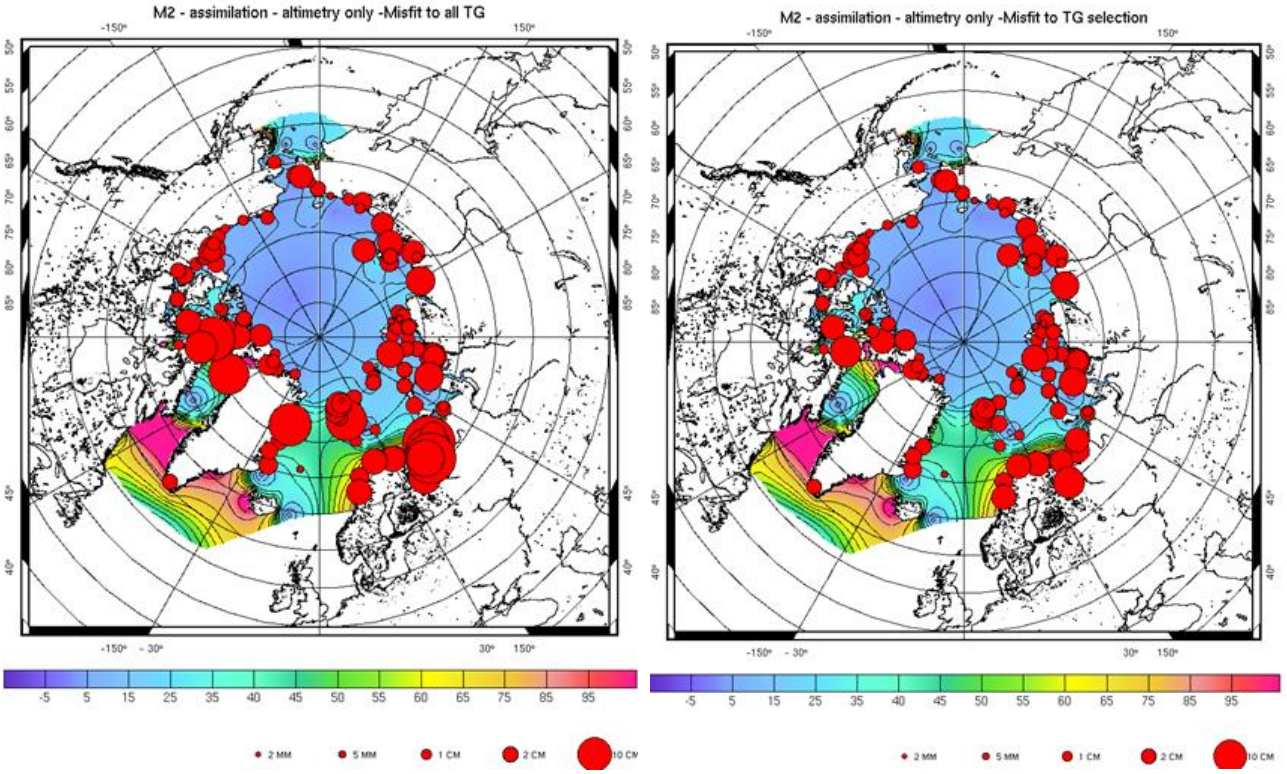

Figure 27: Vector differences (M2 tidal component) between the tide gauge database (all (121 stations) on the left, selection (105 stations) on the right) and the regional tidal model with assimilation of altimetry observations only.

2.5.3. Validation of the optimal tidal atlas

The final and most complete dataset defined for the data assimilation (tide gauge stations and altimetry-derived observations) is presented in Figure 28 and contains 612 observations. For all the tidal components, except K2 (tide gauges only, as mentioned above), the observations assimilated into the model are part of the dataset illustrated in Figure 28.

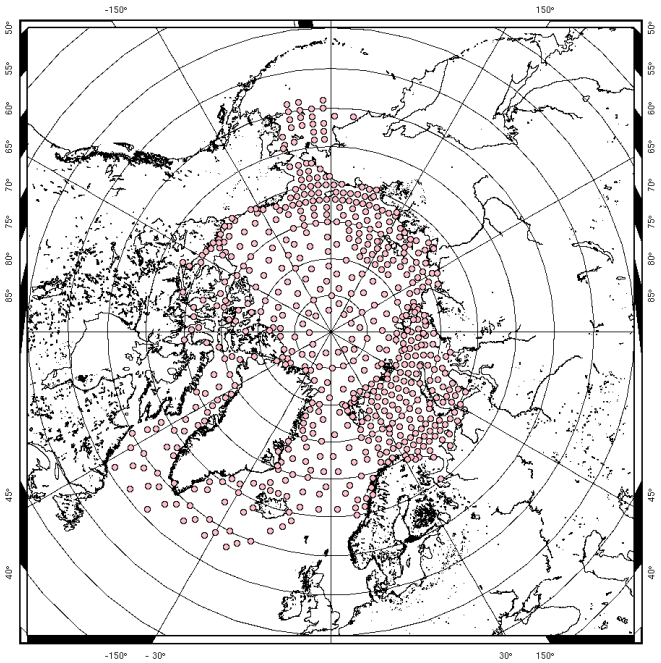

Figure 28: Final assimilation dataset (tide gauge stations and altimetry data) for the M2 tidal component.

The point to keep in mind regarding the validation results presented below is that the data used for the assimilation are included in the validation databases. As a consequence, the validation process is biased compared to an independent validation. However, this analysis gives indications about the efficiency of the data assimilation process and highlights the regions where some specific data selection may be needed. An independent validation would be interesting, but was not planned in the scope of this project. However, regarding the use of the SARAL/AltiKa data, either for data assimilation or validation, the lack of stability of the orbit, which has been drifting for several months, and the lack of maturity on the data both prevent from using this mission for tidal analysis for the moment.

Two databases were used to compute the validation results presented hereafter:

- the tide gauge database before the last editing performed specifically for the assimilation (121 stations);
- the complete altimetry-derived database without decimation (1745 points) computed by DTU Space with the Envisat and CryoSat-2 data.

The validation was done in the frequency domain, for each tidal component, by computing the vector differences between the optimal (i.e. assimilated) regional Arctic model and the validation databases. These vector differences were compared to the results obtained with the competitor global models in the same region and with the same validation databases.

Figure 29 and Figure 30 show the average vector difference computed for each model, for each tidal component, against the tide gauge and the altimetry databases, respectively. As already noted for the validation of the ensemble hydrodynamic simulations in section 2.4, the vector differences are generally higher when comparing to the tide gauge dataset than when comparing to the altimetry dataset. The tide gauge stations are often located in sheltered regions and fjords that are not representative of the open ocean tide, contrary to the altimetry data. In addition, there may be some seasonal artefacts in the comparisons, due to the fact that more tide gauge and altimetry measurements are available in summertime, when there is less sea ice.

The results obtained with the prior hydrodynamic solutions (no data assimilation) of the FES2014 global model ("FES2014 hydro") and the regional Arctic model ("Arctic hydro") are showed for information. It should also be noticed that there was a strong improvement between the FES2012 and the FES2014 global solutions in the Arctic Ocean, as it is highlighted by these comparisons.

The comparison between the "Arctic hydro" solution, in red, and the "Arctic assimilated" solution, in purple, shows the impact of the data assimilation on the regional tidal model. For most of the tidal components (M2, K1...), the improvement due to the assimilation is quite noticeable, for both validation databases. Again, as parts of these

databases have been assimilated in the model (and are strongly correlated with the data that were not assimilated, in the case of the altimetry database), what is highlighted here is the fact that the assimilation worked well and the model was well constrained by the observations, as the differences are reduced. For some components, the improvement is small, but coherent with the amplitudes of these components (Q1).

The comparison to the competitor models highlights a number of points:

- **M2 tidal component:**
  Figure 29 (comparison to the tide gauge database) shows a general improvement of nearly 2 mm for the optimal regional model, compared to FES2014. Both models obtain the best scores with this database, which was used in the assimilation (totally for FES2014, partly for the regional model). The better result obtained by the regional model is consequently due to the higher resolution mesh and to the better physics in the T-UGOm hydrodynamic model. Figure 30 shows a large reduction of the averaged vector difference to the altimetry database for the regional model, compared to FES2014. The FES2014 global model was assimilated with altimetry-derived tidal constituents that were computed at the ERS/Envisat crossover points at the high latitudes and do not benefit from the CryoSat-2 mission specific orbit in the harmonic analysis.
  Figure 31 brings more information to this result as it shows the geographical repartition of the vector differences between the models and the altimetry data. In particular, it appears very clearly on these maps that the main reductions of vector differences in the regional model compared to FES2014 occur in the Baffin Bay, in the North West Passage and on the Siberian shelf.
  Finally, an increase of the vector differences is noticeable in Figure 31 for the regional Arctic model in the southern part of the Baffin Bay. It may be due to the fact that the Hudson Bay was not modeled in the Arctic regional model, as it would demand specific care to obtain an accurate tide solution, such as the implementation of a local tidal model.

- **K1 tidal component:**
  The comparison to both databases shows that the regional tidal model is closer to the observations than its competitor models, for the K1 tidal component. However, it should be reminded here that the annual signal was not perfectly removed from the altimetry sea surface height time series before the computation of the tidal harmonic analysis, which may have particular impact on the K1 estimate derived from the altimetry data. The results in Figure 30 consequently confirm that the data assimilation worked well, as the model is constrained by the altimetry observations and the vector differences are reduced, but that does not mean that the global models have lower performances as the altimetry validation dataset is not the "real truth". However, the regional model also shows good consistency with the tide gauge dataset, which is not impacted by that issue of annual signal retrieval. This thus confirms that the regional K1 solution performs better than the global ones.

- **O1, S2, P1 and Q1 tidal components:**
  These four tidal components show the same kind of results, with a global improvement of the solution thanks to the data assimilation and better performances than the global models, when the differences are significant.

- **K2 tidal component:**
  As previously described, the K2 tidal component had a special treatment regarding the assimilated dataset, with only tide gauge observations, due to the bad quality of the altimetry-derived tidal constituent estimates for this component. This leads to the best solution when comparing to the tide gauge database, and to a solution that is very close to the other models when comparing to the altimetry data. The fact that the vector differences to the altimetry database are very large for all the models, compared to the amplitude of this tidal component (less than 2 cm on average), confirms that the tidal harmonic analysis on the altimetry data was not accurate for this particular tidal component.

- **N2 tidal component:**
  The N2 tidal component also shows different behaviors depending on the validation database. In Figure 30, the vector differences of all the models against the altimetry database are very close and small, around 6 mm. However, the comparison to the tide gauge dataset shows vector differences of generally more than 2 cm, which seems strong compared to the amplitude of this tidal component. In addition, there is a difference of

about 6 mm between the FES2014 model and the regional model compared to the tide gauges, with better performance for FES2014. The maps of the vector differences to the tide gauge database for both models are shown in Figure 32. The main differences between the two models are located along the East coast of Greenland and in the Barents Sea. They systematically occur at tide gauges that were edited during the strict selection performed on the tide gauge database before the assimilation: the Danmarks Havn station on the East coast of Greenland, the Orlov Cape, Morzhovetz Island and Kiya River stations in the Barents Sea. The tidal constituents of these tide gauges were assimilated in the FES2014 global model, but have been eliminated from the assimilation database for the regional model because they were considered as dubious. This is the reason why FES2014 has better performances at these stations (because the data assimilation worked well, once again), and the vector differences are larger for the regional model. As a consequence, this result does not mean that the regional model is of lower quality compared to FES2014. It actually means that the tide gauge data assimilated in the regional model in these regions are not consistent with these four discarded tide gauge stations that show large differences to this assimilated solution, which confirms that these tide gauge stations are dubious.

Globally, all the validation results are coherent and demonstrate the better accuracy of the regional optimal tidal model in the Arctic Ocean, compared to the other available tidal models. Further improvements may still be possible, in particular regarding better retrieval of the annual signal for the diurnal components, but the current solution already shows good performances compared to all its recent global competitors.

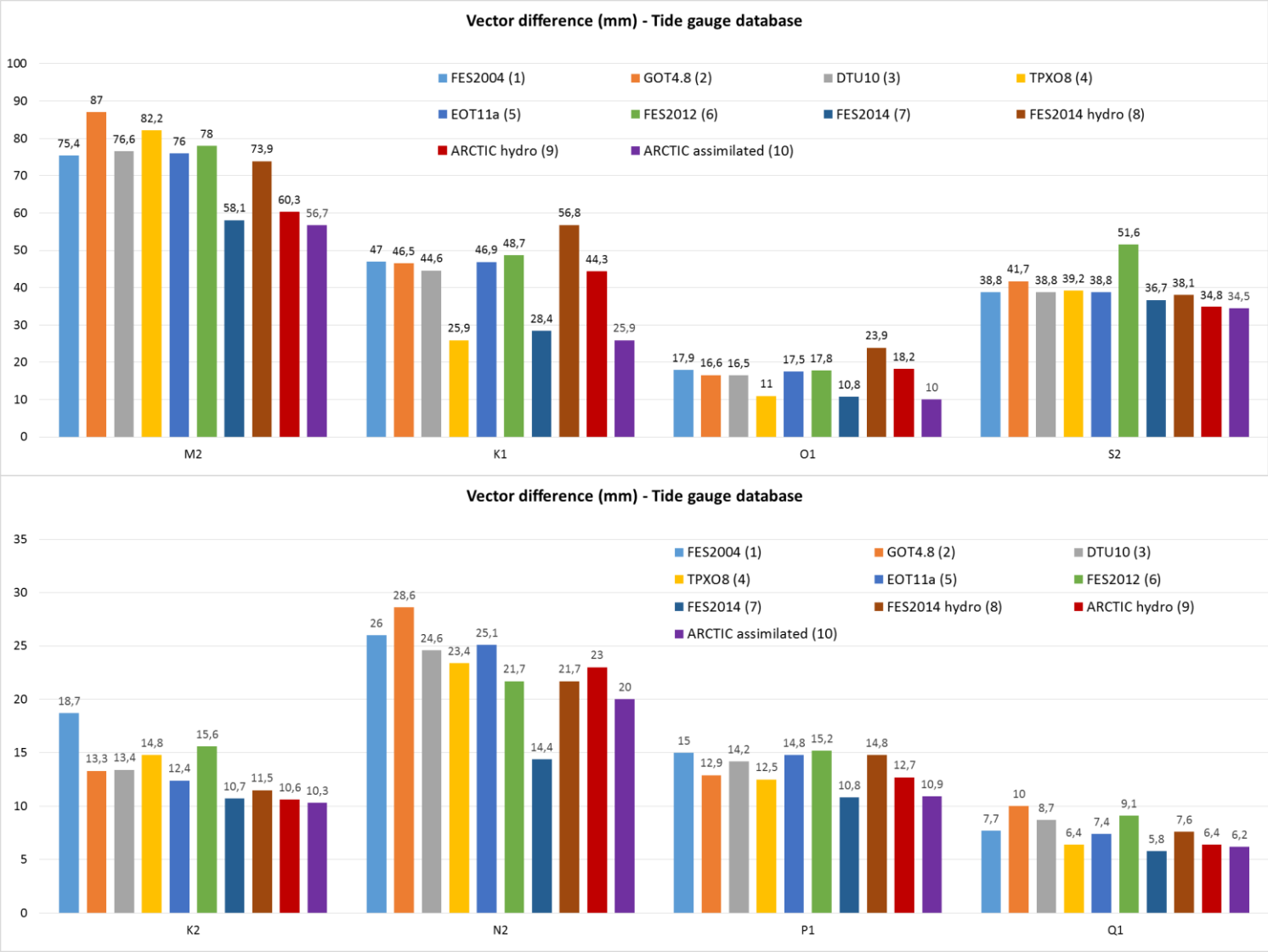

Figure 29: Vector differences between the tidal models and the tide gauge database for each tidal component.

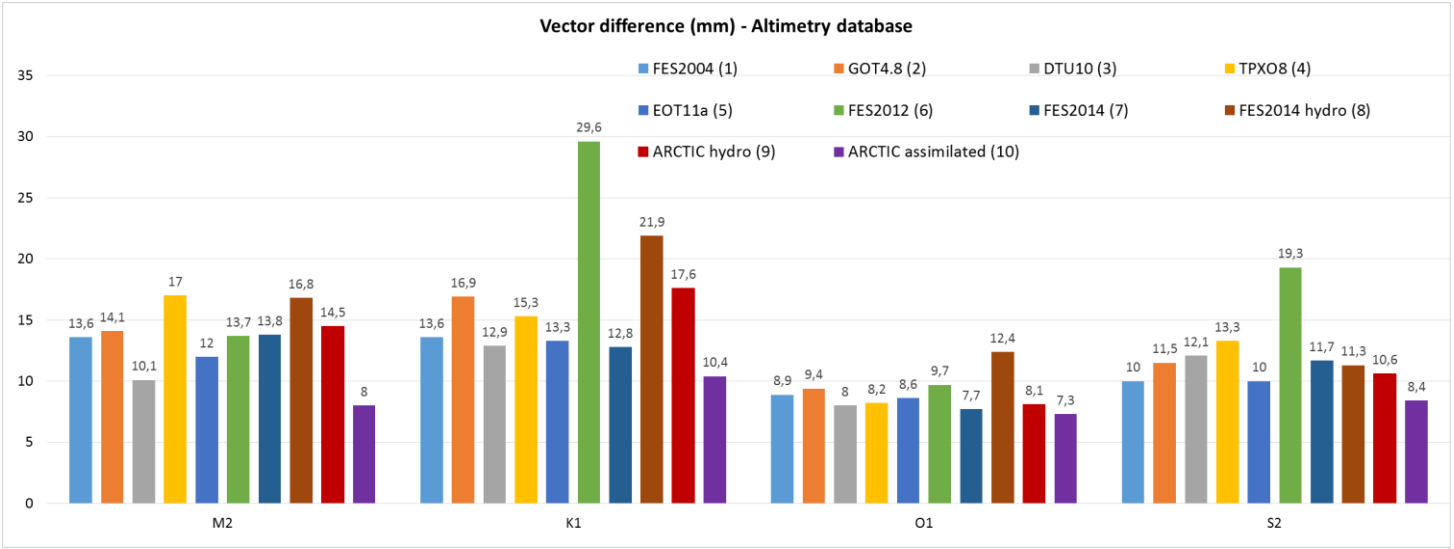

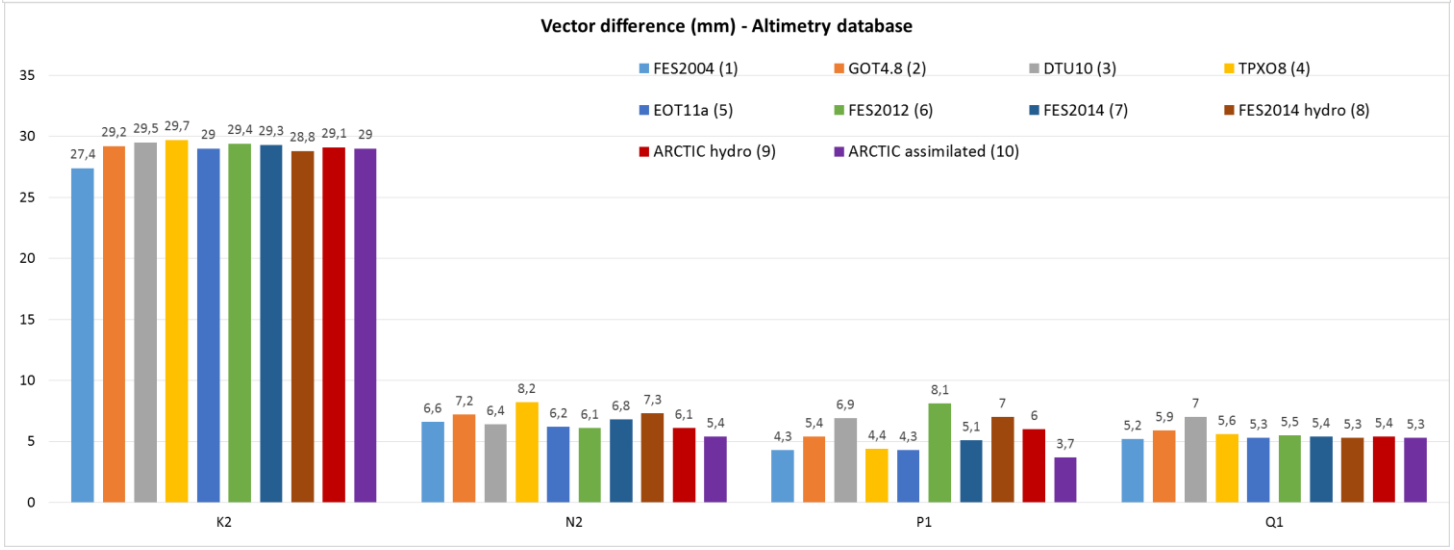

Figure 30: Vector differences between the tidal models and the altimetry database for each tidal component.

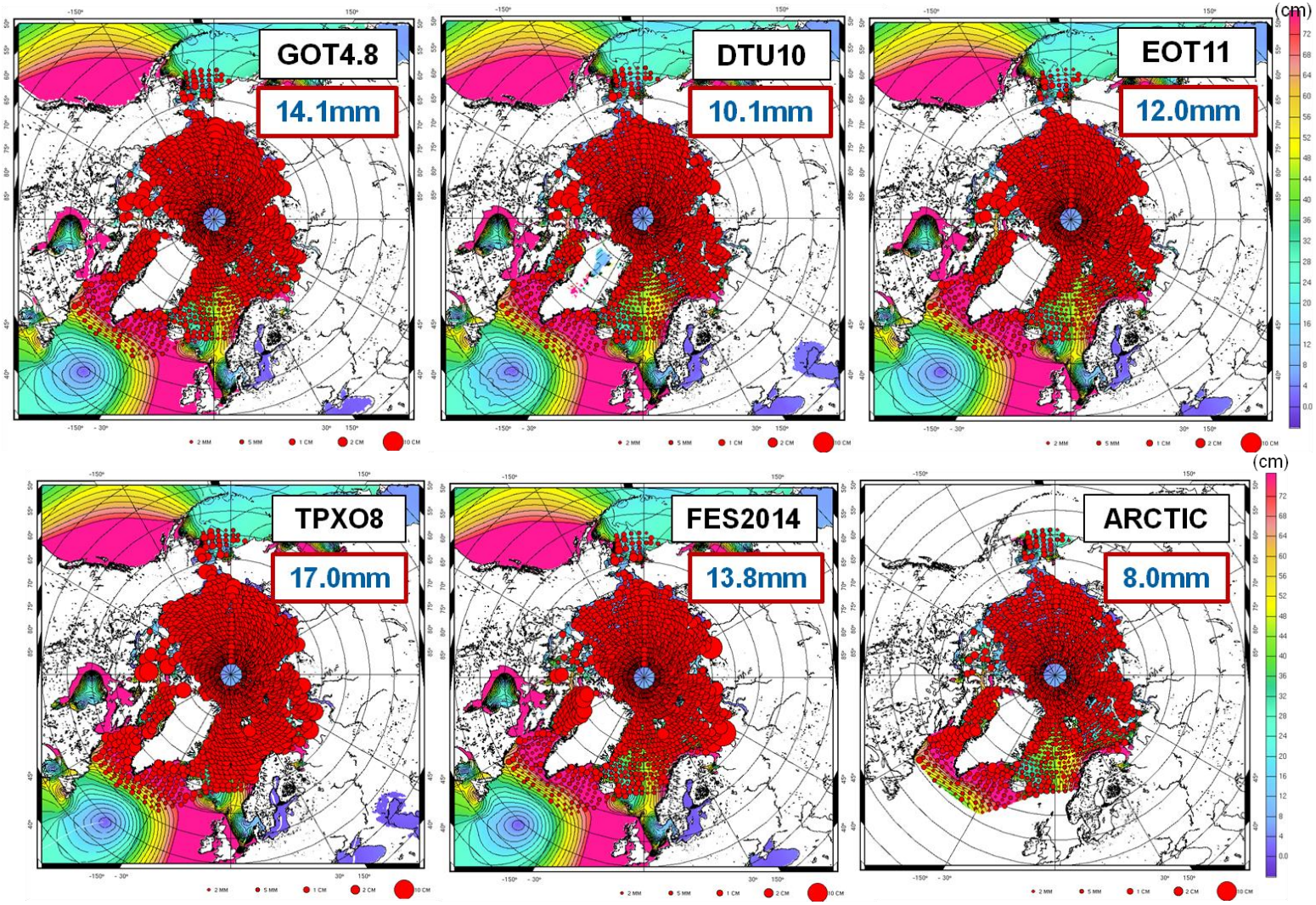

Figure 31: Vector difference between recent global tidal models and the optimal regional model, and the altimetry database for the M2 tidal component in the Arctic Ocean. The value given in blue is the mean vector difference over all the altimetry points. The background colour map is the amplitude of the M2 tidal component from the models (in cm).

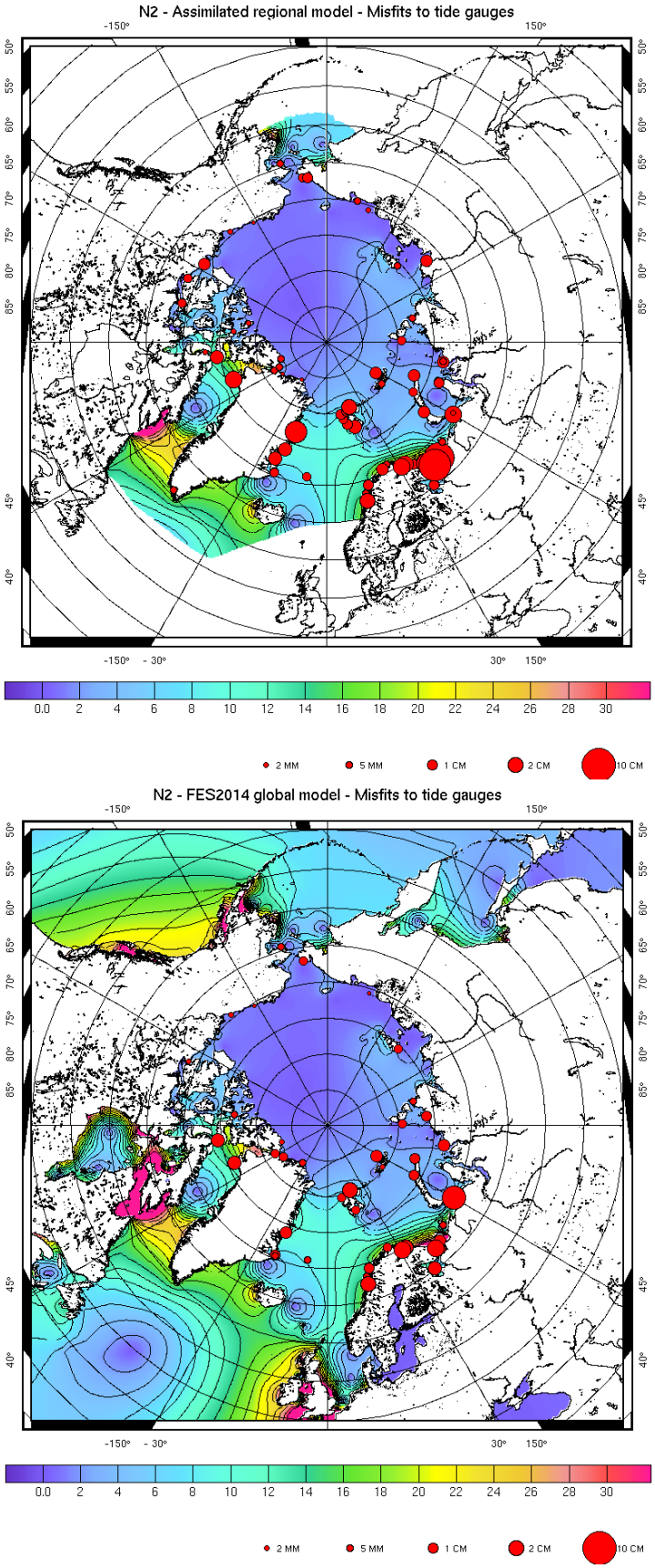

Figure 32: Vector difference between the optimal regional Arctic model (upper plot) and the FES2014 global model (lower plot) respectively, and the tide gauge database for the N2 tidal component. The background colour map is the amplitude of the N2 tidal component (in cm).

3. Conclusions and perspectives

3.1.1. Performances of the Arctic tidal atlas

The validation results demonstrate the high accuracy of the Arctic tidal atlas compared to the most recent global tidal atlases, when the differences are significant.

The good performances of the regional Arctic tidal atlas are due to several factors:

- the fine resolution of the hydrodynamic model unstructured mesh, which has been highly increased compared to the FES2014 global model ;
- the choice of the most appropriate bathymetry dataset available ;
- the physics in the T-UGOm hydrodynamic model that has been locally tuned in order to obtain a prior hydrodynamic solution as close to the observations as possible ;
- the specific processing of the altimetry data (CryoSat-2 and Envisat) performed by DTU Space in order to obtain accurate altimetry-derived tidal constituents ;
- the strict editing of the tide gauge observations ;
- the assimilation of altimetry and tide gauge observations in the a priori hydrodynamic solution.

The regional Arctic tidal atlas has been computed on an unstructured grid with a resolution ranging from a few hundred of meters on the shelves to about 40 km offshore. The atlas contains 8 assimilated tidal components (Semidiurnal: M2, S2, K2, N2. Diurnal: K1, O1, P1 and Q1).

Some additional and independent validation activities will be performed to assess the quality of this regional tidal atlas. If found necessary, the model will be enriched with additional tidal components computed with the time-stepping mode of the T-UGOm hydrodynamic model, which is more adequate to model the non-linear components interactions that are generated mainly on the continental shelves and in the coastal regions [RD3]. No data assimilation would be performed on these additional components as they are too small and of short wavelength to be accurately separated in the altimetry data, and they are not available in the tide gauge dataset.

However, we recommend to use the model “as is” for ocean modeling and forecasting in the Arctic Ocean. It can also provide an improved tidal correction in the CryoSat-2 ocean products, and for altimetry missions with high-inclination orbits, such as Envisat, SARAL/AltiKa and Sentinel-3. The new atlas can also benefit to the Copernicus Marine Environment Monitoring Service (CMEMS), which includes the Arctic Ocean as one of five priority European regional seas, and to other European Arctic observing systems.

Finally, as the Arctic tidal model was built on the basis of the FES2014 global tidal model (FES2014 tidal boundary conditions and regional improvement of the resolution of the FES2014 global mesh), it is possible to integrate the regional model into the global one and obtain a global model with an improved solution in the Arctic Ocean, with perfect match at the boundaries thanks to the unstructured mesh.

3.1.2. Possibilities of improvements

The implementation of the Arctic tidal atlas raised a number of questions regarding the quality of the data used as inputs (bathymetry, coastline, altimetry and tide gauge data) and the physics in the hydrodynamic model. Some possibilities of further improvements have been identified, which could not be implemented or tested in the framework of this study, due to the project planning, the manpower allocation and the availability of the datasets.

- The analysis of the purely hydrodynamic solution (no assimilation) showed that the performances of the main diurnal components (K1 and O1) are lower than the performances of the semi-diurnal components. This is probably due to the definition of the wave drag coefficient (energy transfer between the baroclinic mode and the barotropic mode) in the T-UGOm model. Some possible solutions for improvement have been identified by the LEGOS, where this model is developed, but they would demand some time and some further thinking to be implemented. These defaults have been corrected through the assimilation process, by constraining the model to be close to the observations, but having the best hydrodynamic solution prior to the assimilation would be preferable, in particular in region where the assimilated observations are scarce and sometimes dubious.

- DTU Space identified a source of improvement in the processing of the altimetry data for tidal analysis, regarding the diurnal components. Indeed, the use of a large amount of CryoSat-2 data was thought to be sufficient to enable the discrimination between the annual variation in the sea level and the problem of annual alias periods for the major diurnal constituents for the Envisat sea surface height data, but it is apparently not the case and the derived constituents for several diurnal components (particularly K1 and P1) are not optimally estimated. The problem runs with the alias periods, as shown in Table 1. For CryoSat-2, the alias periods are 112 years for the M2 constituent, infinite for the S2 constituent, 90 years for the K1 constituent and 60 years for the O1 constituent. It was initially thought that the huge amount of CryoSat-2 could help us but apparently the phase of the diurnal constituents changes so slow for CryoSat-2 that this was not the case. Hence, it would be better to initially remove the annual variation in the sea level using a model like the DTU10 annual signal model [RD26], and then use the cleaned signal (better representing the tidal variation in sea level) to estimate the ocean tide parameters. Another source of improvement of the altimetry data would be the computation of error estimates at each point that would help select the accurate data, instead of applying a unique arbitrary error value to all the observations in the assimilation process.

- The bathymetry quality is a crucial point for tidal modeling and the Arctic Ocean is a very complex region on this aspect. The comparisons between two different datasets (IBCAO and R-Topo) showed that they both contain errors. A new version of the R-Topo bathymetry was very recently released, but it was not possible to test it in the framework of this study due to the agenda. However, it would be interesting to make a test with this new dataset, as it is said to have been improved in the Greenland region, where we identified problems in the previous version (see §2.3.4). A complementary approach could consist in designing a specific bathymetry dataset based on these various sources of data. Another strategy could also be the inversion of altimetry data, given the fact that many observations are now available at the high latitudes thanks to the CryoSat-2 mission.

It should be noticed that even if some of these possibilities of improvements demand some developments, this CP4O CCN project was the occasion to automate some tools, such as the mesh generation tools, and to set-up the hydrodynamic model in this specific region. This means that implementing these improvements would not necessarily request to redo the whole work.